Petroleum Science xxx (xxxx) xxx

Contents lists available at ScienceDirect

Petroleum Science

journal homepage: www.keaipublishing.com/en/journals/petroleum-science

Original Paper

Thermal evolution of the Paleozoic in the eastern Sichuan Basin: Insights from thermochronometric analyses and basin modeling

Xin Liu [a,b], Nan-Sheng Qiu [a,b,c,*], Qian-Qian Feng [a,c]

[a] State Key Laboratory of Petroleum Resources and Engineering, China University of Petroleum (Beijing), Beijing, 102249, China
[b] College of Geosciences, China University of Petroleum (Beijing), Beijing, 102249, China
[c] College of Carbon Neutral Energy, China University of Petroleum (Beijing), Beijing, 102249, China

ARTICLE INFO

Article history:
Received 2 August 2024
Received in revised form
16 June 2025
Accepted 21 August 2025
Available online xxx

Edited by Jie Hao and Xi Zhang

Keywords:
Thermal history
Sichuan Basin
Paleozoic source rocks
Emeishan Mantle Plume

ABSTRACT

Eastern Sichuan Basin is a critical region for oil and gas production in China, and the thermal effect of the Emeishan Mantle Plume (EMP) on the basin remains unclear, which limits the study of the Paleozoic hydrocarbon accumulation process. Thus, clarifying the thermal history is crucial for oil and gas evaluation and exploration. This study combines zircon fission track (ZFT), zircon (U-Th)/He (ZHe), and vitrinite reflectance analyses to reconstruct the thermal history since the Paleozoic and investigate the maturity evolution of Paleozoic source rocks in the eastern Sichuan Basin. Additionally, the contributing factors of the Permian abnormal heat flow and the thermal effect range of the EMP were analyzed. Thermal history results show a stable low heat flow phase (45–55 mW/m^2) from the Cambrian to Permian, a rapid increase to peak values (62–70 mW/m^2) during the Middle Permian, and a gradual decline to current stable values (47–62 mW/m^2) from the Triassic onward. Thermal evolution revealed that Paleozoic source rocks exhibited maturation stagnation due to tectonic events, while Permian peak heat flow in the and Jurassic–Late Cretaceous rapid burial accelerated maturation. The Cambrian Qiongzhusi Formation and Silurian Longmaxi Formation source rocks began generating hydrocarbons (R_{equ} = 0.5%) in the Late Cambrian–Late Ordovician and Late Silurian–Early Devonian, respectively, while it was Late Permian–Early Triassic for Permian source rocks. Peak maturity (R_{equ} > 2%) occurred in the Late Cretaceous, with natural gas as the dominant product. The EMP significantly influenced the thermal regime of the western and central Sichuan Basin, with a thermal effect radius of ~600–650 km. In contrast, the Permian thermal anomaly in the eastern Sichuan Basin is attributed to the lithospheric extension associated with the Middle Permian Kaijiang-Liangping trough. These findings provide critical insights for deep and ultra-deep gas exploration and enhance the understanding of the EMP's regional thermal impacts.

1. Introduction

Hydrothermal activity and enhanced heating from Large Igneous Provinces (LIPs) can accelerate the maturation of source rocks, even degrading their hydrocarbon-generating capacity. The Emeishan Large Igneous Province (ELIP), located in the southwest of the Sichuan Basin, linked to the Emeishan Mantle Plume (EMP; Jiang et al., 2023a; Shellnutt, 2014; Zhang et al., 2024), is the most extensively studied LIPs in China. Geochronological data indicate that magmatic emplacement of ELIP occurred over ~4 Ma from 261 to 257 Ma (Huang et al., 2022; Jiang et al., 2023a; Shellnutt et al., 2020). Thermal evolution studies show that the ELIP has profoundly influenced the Permian thermal regime (He et al., 2011; He, 2022; Liu et al., 2018; Qiu et al., 2022; Xu et al., 2018) and the maturation of Paleozoic source rocks in the basin (Feng et al., 2021, 2022; Liu et al., 2018; Qiu et al., 2021, 2022; Zhu et al., 2018). Boreholes in the Sichuan Basin have penetrated the Permian igneous rocks that are geochemically consistent with the ELIP (Li et al., 2017; Liu et al., 2022; Meng et al., 2023). Permian igneous rocks cover an area of 11 × 10^4 km^2 with a thickness exceeding 200 m in the western Sichuan Basin (Ma et al., 2019;

* Corresponding author.
E-mail address: qiunsh@cup.edu.cn (N.-S. Qiu).
Peer review under the responsibility of China University of Petroleum (Beijing).

https://doi.org/10.1016/j.petsci.2025.08.030

Meng et al., 2023; Peng et al., 2022) and less than 80 m in the eastern Sichuan Basin (Feng et al., 2022; Li et al., 2017; Liu et al., 2022; Zhu et al., 2018) (Fig. 1(b)).

Discrepancies persist regarding the spatial extent of the ELIP's thermal effect. Li et al. (2017) estimated a thermal effect radius of 600–700 km, while Jiang et al. (2018) proposed 800–900 km based on paleo-heat flow anomalies. In contrast, numerical simulations by He (2022) constrained the radius to 600–650 km, concluding that the EMP did not influence the eastern Sichuan Basin. These estimates exceed the plume head radius (400–500 km) inferred by He et al. (2006) from erosion thickness analyses of Guadalupian Maokou Formation. Geochemical evidence suggested that the Permian igneous rocks in the eastern Sichuan Basin originated from decompression melting at the plume head's periphery (Liu et al., 2022), implying a potential link to EMP activity. However, geophysical studies identified a hidden hotspot track from the eastern Sichuan Basin to the eruption center (Hu et al., 2023; Liu et al., 2021b). These discrepancies raise critical questions. Did the EMP influence the eastern Sichuan Basin? What mechanisms drove the Permian thermal regime in the eastern Sichuan Basin?

Thermal history studies have revealed the Permian abnormal high heat flow (85–114 mW/m^2) in the western Sichuan Basin, which significantly accelerated the maturation of Paleozoic source rocks (Feng et al., 2021; Qiu et al., 2021, 2022). In contrast, the eastern Sichuan Basin exhibited lower Permian heat flow values (62–75 mW/m^2) (Feng et al., 2021; Qiu et al., 2021, 2022; Zhu et al., 2018). However, Well T1 in the eastern Sichuan Basin penetrated Permian igneous rock and recorded an abnormal high heat flow of 110 mW/m^2 during the Permian (reported by Jiang et al., 2018; Zhu et al., 2018). Feng et al. (2022) inferred that the abnormal heat flow accelerated the maturation of Paleozoic source rocks. Conversely, other studies argued that no such high heat flow event occurred in the eastern Sichuan Basin, with no discernible impact on Paleozoic source rocks maturity (Liu et al., 2023, 2024; Qiu et al., 2022).

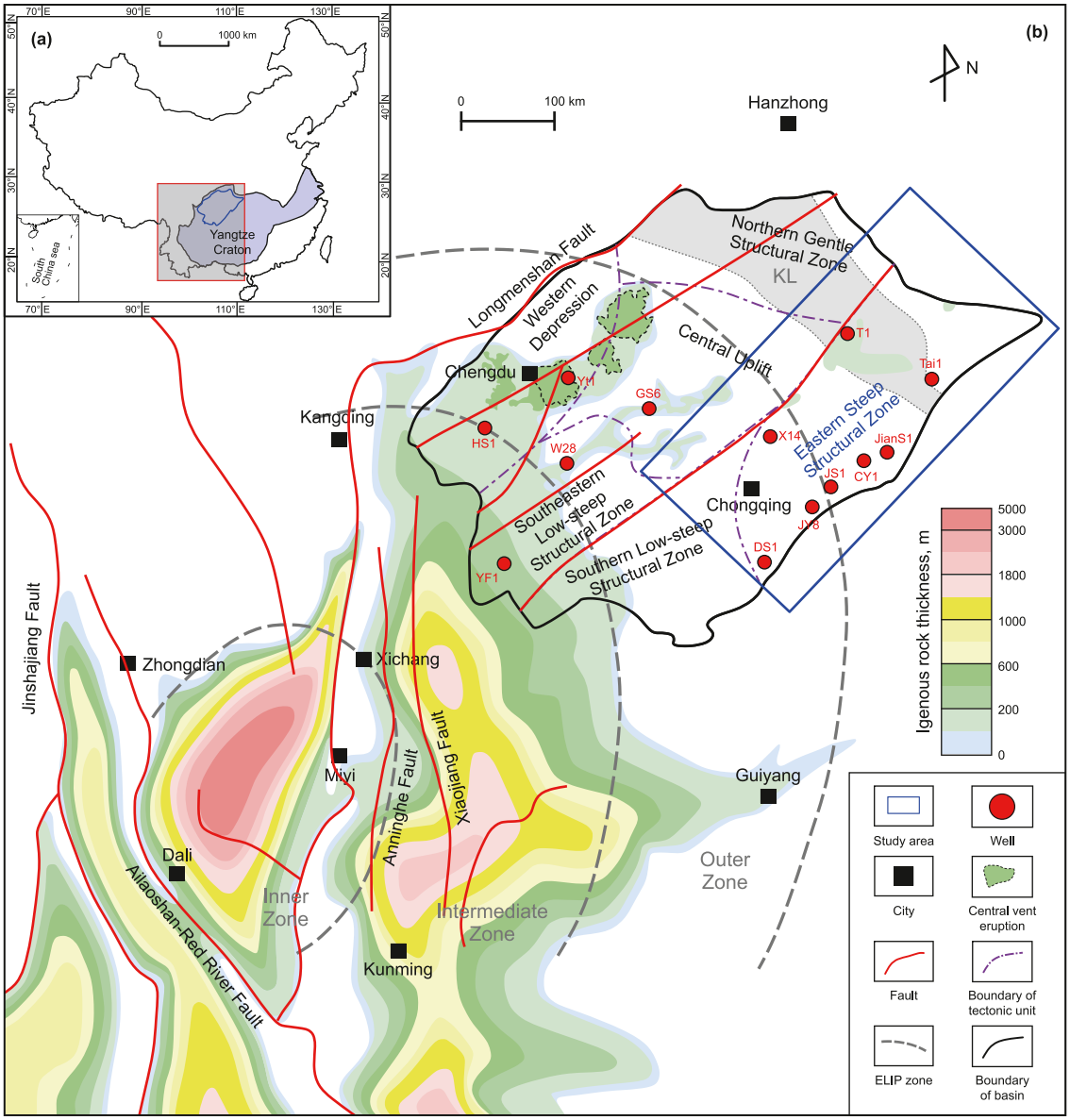

Fig. 1. (a) Tectonic location of the Sichuan Basin. **(b)** Schematic map of the ELIP and tectonic zoning of the Sichuan Basin (modified after Meng et al., 2023). The inner, intermediate, and outer zones in the ELIP are defined by He et al. (2006) and Li et al. (2017). The Permian volcanic rock distribute in the Sichuan Basin are modified after Ma et al., (2019). KL: Kaijiang-Liangping trough.

These conflicting interpretations highlight persistent uncertainties, whether Permian abnormal high heat flow existed in the eastern Sichuan Basin, and the potential role in the thermal evolution of Paleozoic source rocks. Resolving these questions is critical for understanding the hydrocarbon generation processes in deeply buried, highly matured source rocks and advancing exploration strategies for deep and ultra-deep gas resources.

This study reconstructs the thermal history of the eastern Sichuan Basin since the Paleozoic using zircon fission track (ZFT), zircon (U-Th)/He (ZHe) and vitrinite reflectance analyses, and obtains the thermal history of typical wells in the study area. Based on the thermal history, we clarify the maturity evolution of the Paleozoic source rocks, analysis the contributing factors of the Permian abnormal heat flow and the spatial extent the of EMP's thermal effect, discuss the different influences of the EMP on the Paleozoic source rocks in the Sichuan Basin. Finally, we propose a conceptual geodynamic model to explain the origin of the Permian thermal regime in the eastern Sichuan Basin. This study advances the exploration of deep to ultra-deep gas resources in the Sichuan Basin and provide a novel insight into the thermal effect of ELIP.

2. Geological background

The Sichuan Basin is a large petroliferous basin located in the Yangtze Block, with an area of 2.6×10^5 km^2 (Dai et al., 2021) (Fig. 1(a)). Current geothermal gradients range from 17.7 °C/km to 33.4 °C/km, with the average of 22.7 °C/km, and terrestrial heat flow values of 40–70 mW/m^2 with average of 53.8 ± 7.6 mW/m^2 (Jiang et al., 2019; Qiu et al., 2022; Zhu et al., 2022). Notably, the eastern Sichuan Basin exhibits relatively lower heat flow, about 40–55 mW/m^2, increasing gradually from the northeast to southwest (Cao et al., 2015; Zhu et al., 2017). Structurally, the basin is divided into the northern gentle structural zone, the central uplift, the southwestern gentle low-steep structural zone, the southern gentle low-steep structural zone, the western depression, and the eastern steep structural zone (Fig. 1(b)). The study focuses on the eastern steep structural zone, bounded by the Huayinshan Fault to the west and the Dabashan Tectonic Belt to the north (Fig. 2(a)).

Multiple tectonic movements have shaped the basin's evolution. The Tongwan movement triggered extensive uplift and denudation in the Late Sinian (Liu et al., 2021a). The Caledonian Movement in the Late Silurian resulted in significant denudation of Devonian–Carboniferous strata, with a thickness of 1200–1400 m in the central and western zones and 200–400 m elsewhere (Xu et al., 2018; Yuan et al., 2013). The Dongwu Movement in the Permian induced crustal uplift in the Yangtze Block, with denudation decreasing westward in the Sichuan Basin, with thickness of 100–200 m in the study area (Zhu et al., 2009). In the late Triassic, the Indosinian Orogeny further modified the basin's architecture (Zhu et al., 2009). In the Late Cretaceous, the Yanshan-Himalayan Movement caused intense denudation of 3000–4500 m (Feng et al., 2023; Zhu et al., 2017).

Geochronology and geochemistry evidences suggest that the South Qinling Ocean, located in the northern margin of the Yangtze Block, underwent eastward expansion and subduction beneath the North China Block during the Late Carboniferous to Early Triassic (Cheng et al., 2022; Dong et al., 2021; Wang et al., 2024). This process established a passive continental margin, placing the Sichuan Basin in a pronounced extensional tectonic regime (Xu et al., 2021b; Xiao et al., 2023; Zhang et al., 2022). During the Middle Permian, the EMP impinged on the Yangtze Block. The Yangtze Block experienced significant thermal perturbations during the Permian due to ELIP, which elevated heat flow in the Sichuan Basin to ~85–114 mW/m^2 (Feng et al., 2021, 2022; He et al., 2011; Qiu et al., 2022). The ELIP spans an area of 2.8×10^5 km^2 across Sichuan, Yunnan, and Guizhou provinces along the western margin of the Yangtze Block, SW China (Fig. 1(b)). Bounded by the Longmenshan Fault to the northwest and the Ailaoshan-Red River Fault to the southwest (Shellnutt, 2014). The ELIP is widely attributed to mantle plume activity (Zhang et al., 2024). It is divided into outer, intermediate, and inner zones (Fig. 1(b)) (He et al., 2006). Geochronological, paleontological, and paleomagnetic data indicate that magmatism of ELIP emplaced in a main pulse of ~4 Ma from ~261 Ma to ~257 Ma, with protracted activity spanning ~17 Ma (Huang et al., 2022; Jiang et al., 2023a; Shellnutt, 2014; Shellnutt et al., 2020; Xu et al., 2021a; Zhu et al., 2021). Permian igneous rocks buried within the Sichuan Basin are concentrated in the southwestern region, the Jianyang-Santai area, and the eastern region, with thicknesses decreasing westward to eastward from 80–300 m to 20–65 m (Fig. 1(b)) (Ma et al., 2019). These rocks unconformably overlie the Maokou Formation and underlie the Longtan Formation (Fig. 2(b)). Geochemical and geophysical evidence confirms their genetic linkage to the ELIP (Hu et al., 2023; Li et al., 2017; Liu et al., 2021b, 2022).

The Paleozoic strata in the eastern Sichuan Basin are predominantly composed of marine carbonate rocks and shales interbedded with minor clastic deposits, with erosional removal of Upper Silurian, Middle-Upper Devonian, and Upper Carboniferous strata (Fig. 2(b)). Well-developed Paleozoic marine source rocks in this region include the Upper Permian Longtan Formation, Middle Permian Qixia-Maokou Formation, Lower Silurian Longmaxi Formation, and Lower Cambrian Qiongzhusi Formation (Fig. 2(b)) (Dai et al., 2021; Jiang et al., 2023b; Li et al., 2021; Sun et al., 2021). The Upper Permian Longtan Formation, widely distributed across the basin, comprises coal seams and dark shales with a thickness of 50–160 m (Chen et al., 2018a; Liu et al., 2015). These rocks exhibit high total organic carbon (TOC >2%) and abundant sapropelic organic matter (Chen et al., 2018b; Li et al., 2021; Liu et al., 2015; Luo et al., 2019). The Middle Permian Qixia-Maokou Formation in the eastern Sichuan Basin consists of marlstone-dominated lithologies, with a thickness of 50–200 m, and the TOC values ranging from 0.3% to 3.0%, with an average of 0.8% (Chen et al., 2018b; Chen et al., 2023). The Lower Silurian Longmaxi Formation, predominantly developed in the eastern and southern regions, features black shales and mudstones averaging 203 m in thickness (Hong et al., 2020; Jiang et al., 2023b; Zhao et al., 2023). It is classified as a good-high quality source rock due to its elevated TOC (1.0%–4.0%, average 1.52%) and dominance of Type I kerogen (Hong et al., 2020; Jiang et al., 2023b; Sun et al., 2021). The Lower Cambrian Qiongzhusi Formation comprises dark mudstones and shales (30–150 m thick) with sapropelic organic matter in the study area (Jiang et al., 2023b; Li et al., 2021; Qiu et al., 2021; Sun et al., 2021).

3. Samples and methods

3.1. Samples

This study employed ZFT, ZHe, and R_{equ} analyses to reconstruct the thermal history. For natural evolution samples in the sedimentary basins, the partial annealing zone (PAZ) temperature ranges of ZFT and ZHe are 170–390 °C (Yamada et al., 1995, 2007) and 140–200 °C (Cai et al., 2020), respectively. These methods are particularly suitable for reconstructing the thermal history of deeply buried, ancient strata.

Due to the absence of exposed Lower Paleozoic strata in the eastern Sichuan Basin and the ease of separating zircon from clastic rocks, five outcrop samples were collected from the periphery of the basin. These include clastic rocks from the Lower Cambrian Canglangpu Formation, Lower Ordovician Meitan

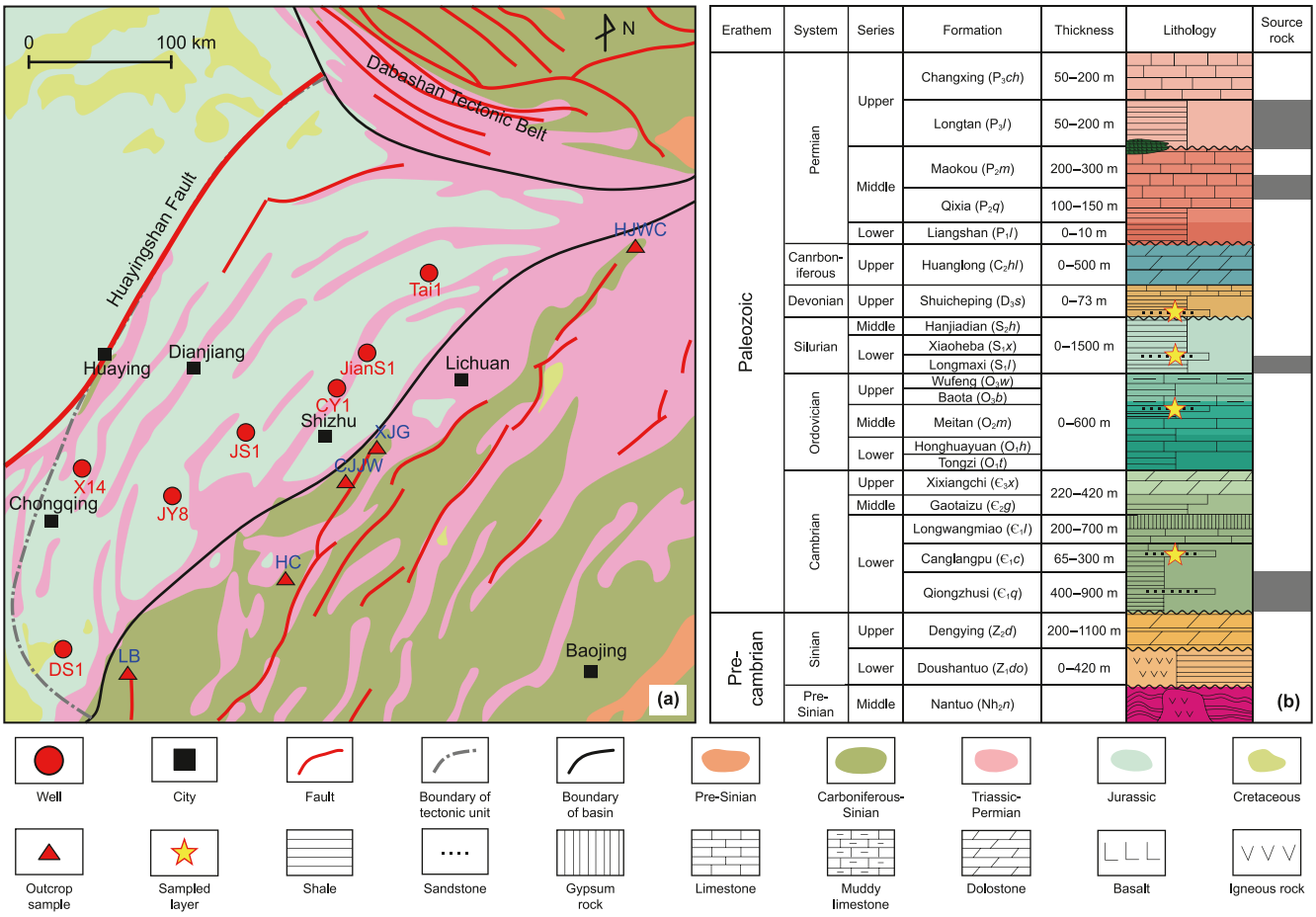

Fig. 2. (**a**) Geological map and samples distribution in the eastern Sichuan Basin (modified after Zheng et al., 2017). **(b)** General stratigraphic column and source rocks of the eastern Sichuan Basin (modified after Feng et al., 2022; Li et al., 2023).

Formation, Lower Silurian Xiaoheba Formation and Upper Devonian Shuicheping Formation at the periphery of the basin (Fig. 2 (a)–Table 1). The ZFT analysis was omitted for Sample CJJW due to insufficient zircon grains. Unexpectedly, apatite was identified during mineral separation for sample XJG, prompting additional apatite fission track (AFT) analysis.

3.2. Fission track

The AFT and ZFT analyses were performed in the State Key Laboratory of Petroleum Resources and Engineering, China University of Petroleum (Beijing). After mineral separation, apatite and zircon grains were prepared as targets through grinding and polishing to expose crystal surfaces. Etching protocols were rigorously applied to reveal fission tracks: apatite targets were treated with 5.5 mol/L HNO_3 at 21 ± 0.5 °C for 20 s, while zircon targets were etched using a 1:1 KOH-NaOH mixture at 228 °C for 12 h. After etching, density of spontaneous fission tracks (ρ_s) were measured by TrackWorks 3.0 software under a microscope. Uranium (U) concentrations within the track regions were quantified via laser ablation inductively coupled plasma mass spectrometry (LA-ICP-MS), and original data processing utilized Iolite 4.0 (Paton et al., 2011). The fission track ages were calculated by IsoplotR (Vermeesch, 2018).

3.3. Zircon (U-Th)/He

The ZHe analyses were conducted at two facilities: The State Key Laboratory of Petroleum Resources and Engineering, China University of Petroleum (Beijing), and the $^{40}Ar/^{39}Ar$ and (U-Th)/He chronology laboratory of the Institute of Geology and Geophysics, Chinese Academy of Sciences. Euhedral zircon grains exceeding 60 μm in diameter were selected, and their physical characteristics (length, width, height, cone length, morphology, cracks, and

Table 1
The strata, lithology, elevation and location of the outcrop samples.

No.	Sample	Strata	Lithology	Elevation, m	Longitude-latitude	Analysis methods
1	CJJW	$Є_1c$	Muddy siltstone	1701	N29°47′15″, E108°15′02″	ZHe
2	LB	O_1m	Muddy siltstone	595	N28°53′11″, E106°56′00″	ZFT, ZHe
3	HC	S_1x	Siltstone	245	N29°20′17″, E107°56′26″	ZFT, ZHe
4	XJG	S_1x	Siltstone	1280	N29°53′03″, E108°17′18″	AFT, ZFT, ZHe
5	HJWC	D_3s	Quartz sandstone	384	N31°03′28″, E109°57′35″	ZFT, ZHe

inclusions) were documented. Selected grains were encapsulated in 1 mm × 1 mm niobium capsules and analyzed for helium content using the Alphachron MK II helium extraction instrument. After that, the capsules were transferred into Teflon bottles, where they were digested in a mixture of concentrated hydrofluoric acid (HF) and a diluent solution containing known concentrations of ^{235}U and ^{230}Th. Multiple digestion cycles in the autoclaves ensured complete dissolution. The resulting solutions were evaporated to dryness, mixed with ultrapure water, and analyzed for uranium (U) and thorium (Th) concentrations via ICP-MS. (U-Th)/He ages were calculated using HelioPlot (Vermeesch, 2010) and corrected following the method of Gautheron & Tassan-got. (2010).

3.4. Organic matter paleothermometers

Organic matter paleothermometers, including vitrinite reflectance (R_o) and equivalent vitrinite reflectance (R_{equ}), are the most commonly used in the thermal history reconstruction. The vitrinite reflectance (R_o), bitumen reflectance (R_b), and vitrinitelike reflectance (R_v) data of typical wells (Well X14, DS1, JY8, CY1, JianS1, Tai1, and JS1) were obtained from previous researches (Feng et al., 2021, 2023; Jiang et al., 2018; Li et al., 2021; Liu et al., 2023; Qiu et al., 2021; Wang et al., 2022; Zhu et al., 2017, 2018), and R_b and R_v had been calculated to R_{equ} with the corresponding empirical formulae (Petersen et al., 2020; Schmidt et al., 2019; Wu et al., 2023a).

4. Results

4.1. Fission track

The AFT results of sample XJG are summarized in Table 2, yielding a central age of 44.9 ± 3.6 Ma and a mean track length (MTL) of 10.98 ± 2.30 μm (Fig. 3). The high P(χ^2) value (>0.05) and low age dispersion (<15%) indicate that the apatite grains underwent the same thermal history. The central age is significantly younger than the stratigraphic age, indicating that the peak paleogeothermal temperature exceeded the AFT annealing temperature (>120 °C), resulting in full resetting of the fission track system.

The ZFT data are summarized in Table 2, with central ages ranging from 277.8 ± 37.9 Ma to 335.3 ± 35.1 Ma. These ages are consistently younger than their respective stratigraphic ages (Table 2), indicating post-depositional annealing. The low P (χ^2) values (<0.05) and high age dispersions (>15%) suggest heterogeneous grain-age populations, with ages resolving into 2 to 4 distinct peaks (Fig. 4). Samples LB, HC, and XJG exhibit two peaks at 275.7 ± 36.0 Ma and 445.9 ± 55.7 Ma, 193.2 ± 29.8 Ma and 497.4 ± 55.1 Ma, and 209.3 ± 25.4 Ma and 398.9 ± 44.9 Ma, respectively. Sample HJWC reveals four peaks at 19.9 ± 56.6 Ma, 225.6 ± 47.3 Ma, 366.8 ± 34.1 Ma, and 565.2 ± 63.6 Ma. These peaks correlate with major tectonic events in the Sichuan Basin: the Sinian–Early Cambrian Tongwan movement (565.2 ± 63.6 Ma–497.4 ± 55.1 Ma), Silurian–Late Devonian Caledonian movement (445.9 ± 55.7 Ma–366.8 ± 34.1 Ma), Middle Permian Dongwu movement (275.7 ± 36.0 Ma), Late Triassic Indosinian orogeny (225.6 ± 47.3 Ma–209.3 ± 25.4 Ma), and Jurassic–Early Cretaceous Yanshan-Himalayan movement (193.2 ± 29.8 Ma–119.9 ± 56.6 Ma). A significantly negative correlation between single-grain ZFT ages and uranium contents (Fig. 5) suggests that radiation damage in zircon grains likely contributed to the age dispersion.

4.2. Zircon (U-Th)/He

The ZHe data are presented in Table 3. Single-grain ZHe ages range from 91.9 ± 1.1 Ma to 279.7 ± 4.5 Ma, significantly younger than their stratigraphic ages. This discrepancy indicates helium diffusion during the peak paleo-geothermal temperatures or maximum burial conditions, with peak temperatures exceeding the ZHe annealing temperature (200 °C). The observed age dispersion is attributed to radiation damage effects, as evidenced by a pronounced negative correlation between single-grain ZHe ages and effective uranium concentrations (eU) (Fig. 6(a)). In contrast, no correlation exists between ages and grain radii (Fig. 6 (b)), consistent with radiation-induced lattice defects rather than crystal size controlling helium retention (Flowers et al., 2009; Gautheron et al., 2013).

4.3. Vitrinite reflectance

The R_{equ} values range from 0.55% to 4.60%, exhibiting a broadly linear positive correlation with depth (Fig. 7). In this study, the maturity of source rocks can be divided into six stages, the immature (R_{equ} < 0.5%), early mature (0.5% < R_{equ} < 0.7%), middle mature (0.7% < R_{equ} < 1.0%), late mature (1.0% < R_{equ} < 1.3%), main gas generation (1.3% < R_{equ} < 2.6%), and over-mature (R_{equ} > 2.6%).

5. Thermal evolution of the eastern Sichuan Basin

5.1. Thermal history modeling

The thermal modeling was invert by the Hefty software with the Monte Carlo approach. The fanning curvilinear model was used for the AFT data (Ketcham et al., 2007), the parallel curvilinear model was used for the ZFT data (Yamada et al., 2007), and the radiation damage accumulation and annealing model was used for ZHe data (Guenthner et al., 2013). Initial and current temperatures were 20 ± 5 °C, while tectonic movement timings and erosion amounts served as constraints. A total of 10^3–10^5 time-temperature (t-T) paths were simulated. Results for the five clastic rock samples (Fig. 8) reveal four heating-cooling phases since the Cambrian: (1) The Early Cambrian – Late Silurian heating, followed by the Late Silurian – Late Carboniferous cooling about 10 °C linked to the Caledonian movement; (2) The Late Carboniferous – Middle

Table 2
The measured fission track ages.

Analysis methods	Sample	Grain No.	ρ_s, 10^5/cm^2	Ns	U, ppm	P(χ^2)	Central age±2σ, Ma
AFT	XJG	23	24.7	624	80.3	0.45	44.9 ± 3.6
ZFT	LB	33	110.0	958	162.6	0	335.3 ± 35.1
	HC	26	115.5	882	172.9	0	304.2 ± 65.5
	XJG	32	100.3	1146	129.8	0	277.8 ± 37.9
	HJWC	62	108.4	2990	117.1	0	291.8 ± 34.1

Note: ρ_s represent density of spontaneous tracks. Ns represent the sum of spontaneous fission-tracks. U is the mean uranium concentration. P(χ^2) is chi-square probability. The central ages are calculated by IsoplotR (Vermeesch, 2018).

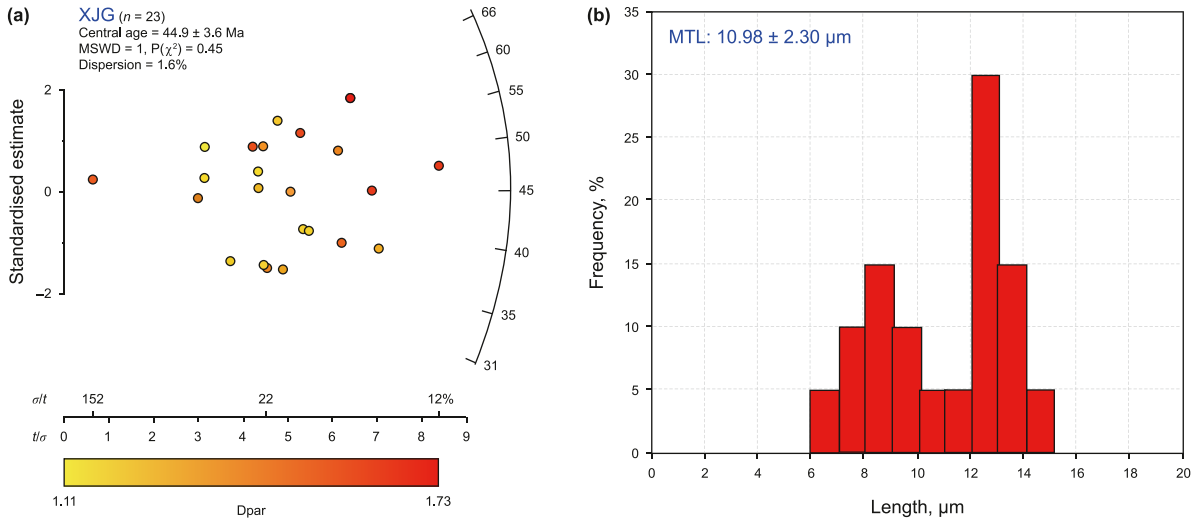

Fig. 3. (**a**) The radial plot AFT data of sample XJG. **(b)** detrital apatite fission track lengths of AFT data of sample XJG. MTL is the mean track length of the detrital apatite.

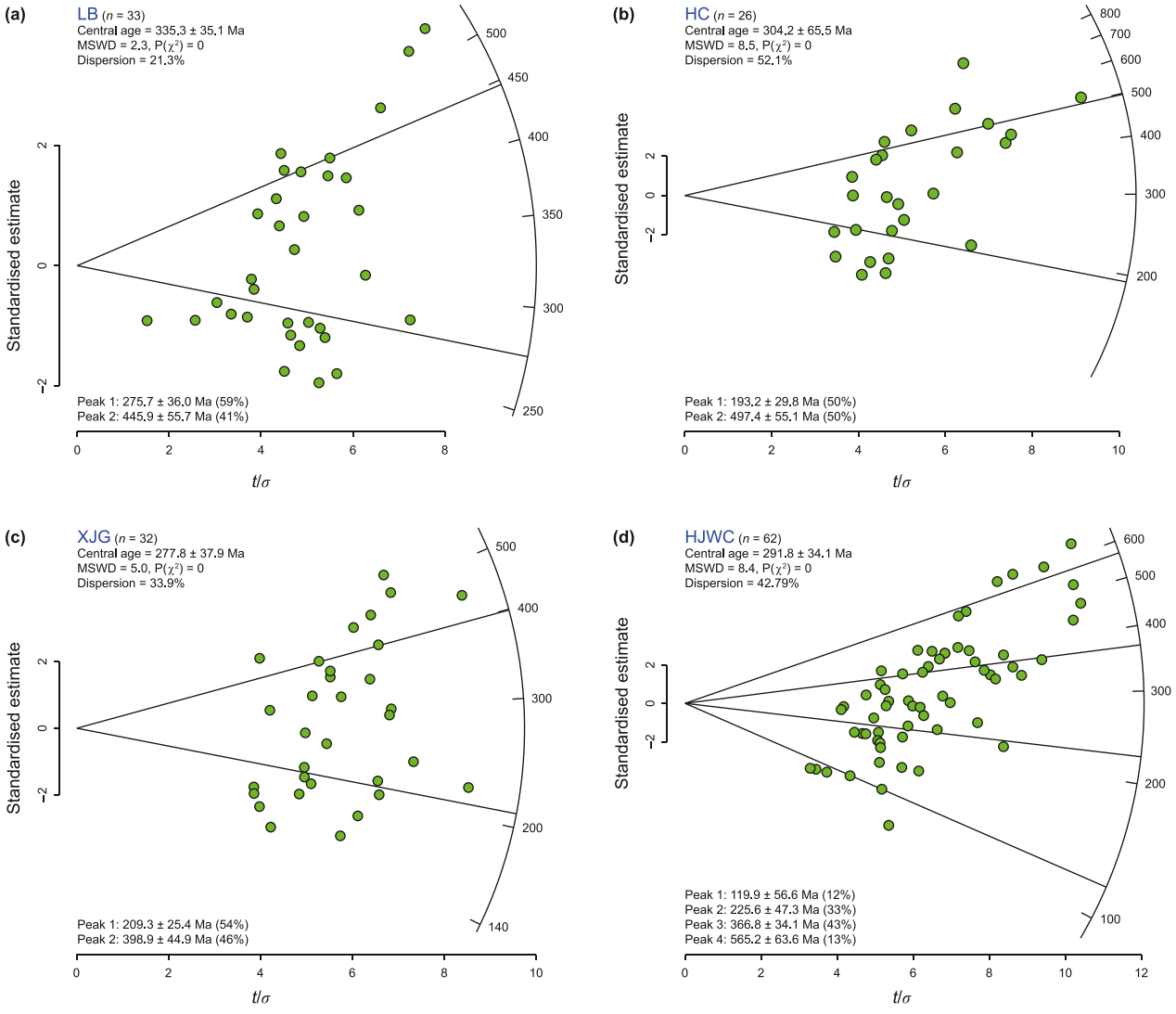

Fig. 4. The radial plots of ZFT data of samples, showing the central and peak ages. The detrital ZFT age were divided into two to four peaks for samples using the IsoplotR, respectively (Vermeesch, 2018). The P(χ^2) values of the samples were zero and the percentage dispersions were greater than 15%, indicating a mixture of components with different grain-ages.

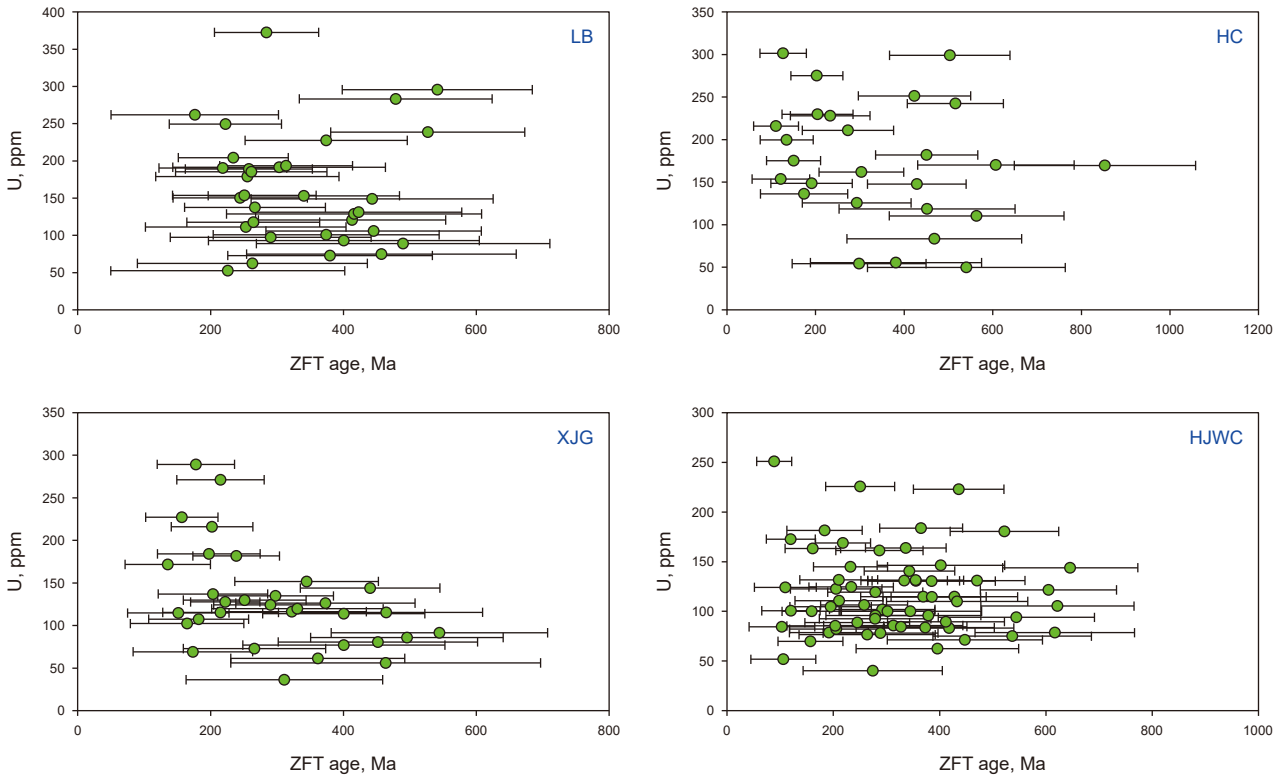

Fig. 5. The relationship between the ZFT single-grain ages and uranium content. The ZFT single-grain ages were inversely correlated with their U concentrations, indicating different radiation damage resulted in differences in the annealing temperature and ZFT single-grain ages.

Table 3
The measured ZHe ages.

Grain No.	Radius, μm	^{4}He, nmol·g^{-1}	Mass, μg	Ft	U, ppm	Th, ppm	eU, ppm	Corrected age±1σ, Ma
CJJW, Lower Cambrian muddy siltstone								
1	41.6	53.8	2.3	0.73	80.7	94.9	103.0	132.4 ± 1.7
2	41.2	57.6	2.0	0.73	42.4	39.8	51.8	279.7 ± 4.5
3	43.5	66.7	2.4	0.74	103.4	89.8	124.5	133.2 ± 1.9
4	34.0	45.7	1.2	0.67	87.6	115.4	114.7	109.7 ± 1.5
LB, Middle Ordovician muddy siltstone								
1	37.5	95.7	1.5	0.71	182.2	68.1	198.2	125.9 ± 1.9
2	40.5	49.4	1.9	0.73	140.7	53.7	153.3	81.9 ± 1.1
3	36.2	102.3	1.4	0.70	170.8	64.1	185.9	145.5 ± 2.0
HC, Lower Silurian siltstone								
1	38.4	29.4	1.8	0.70	43.5	51.5	55.6	138.2 ± 1.8
2	38.3	39.6	1.7	0.71	68.3	36.5	76.9	133.6 ± 2.0
3	35.4	237.6	1.3	0.69	446.5	198.9	493.2	128.9 ± 2.1
4	36.0	123.8	1.5	0.69	254.0	83.1	273.5	120.1 ± 1.8
XJG, Lower Silurian siltstone								
1	40.9	55.5	2.0	0.73	129.1	24.9	134.9	103.9 ± 1.6
2	40.9	89.0	2.0	0.73	169.9	51.6	182.0	123.6 ± 1.9
3	42.3	161.6	2.26	0.73	301.1	226.7	354.4	114.5 ± 1.9
4	39.5	124.6	1.8	0.72	226.9	85.9	247.1	129.1 ± 2.0
HJWC, Upper Devonian quartz sandstone								
1	65.4	83.2	8.4	0.82	144.8	80.6	163.7	113.4 ± 1.7
2	64.9	44.3	9.1	0.82	50.3	53.5	62.8	157.7 ± 2.0
3	63.1	91.4	9.5	0.82	153.7	80.6	172.6	119.0 ± 1.6

Note: Ft: alpha correction factor (Ketcham et al., 2011); eU: effect uranium concentration, eU = U+0.235Th (Flowers et al., 2007).

Permian heating, succeeded by the Middle Permian – Early Triassic cooling (~10–15 °C) during the Dongwu movement; (3) The Early Triassic – Late Triassic heating, with subsequent the Late Triassic – Early Jurassic cooling ~ 10–20 °C driven by the Indosinian movement. (4) The Late Cretaceous thermal peak, where maximum paleotemperatures reached 260–280 °C for Cambrian strata, 230–260 °C for Ordovician strata, 220–260 °C Silurian strata, and 200–240 °C for Devonian strata. Post-Cretaceous cooling, attributed to the Yanshan-Himalayan movement.

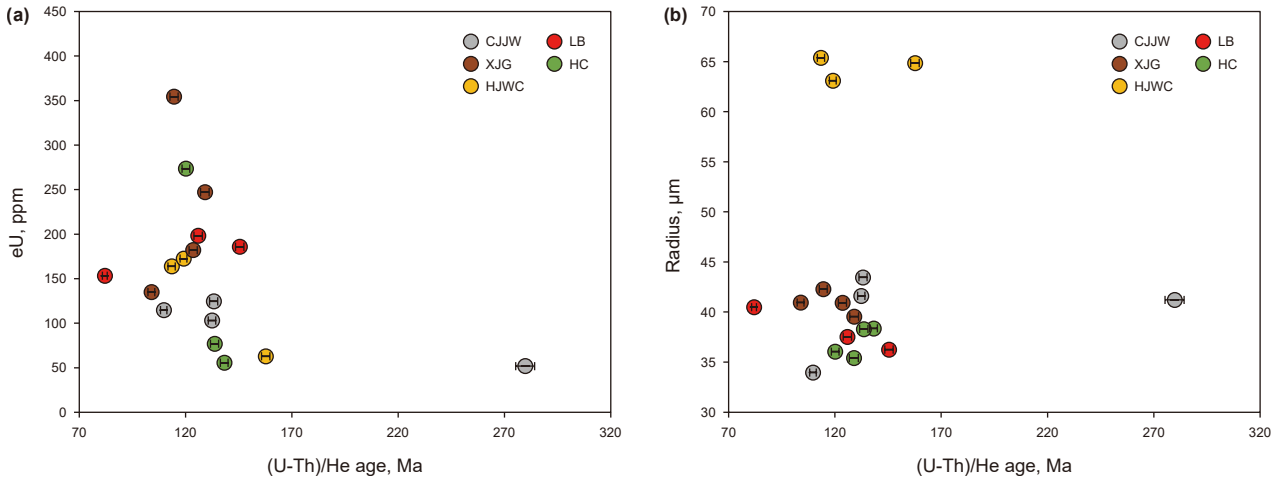

Fig. 6. (**a**) The correlation of eU with ZHe single-grain ages. **(b)** The correlation of radius with ZHe single-grain ages. There is no clear relationship between ZHe ages and radiuses. The samples with the higher eU values have the younger ages, indicating that radiation damage results from the dispersion of the ZHe single-grain ages.

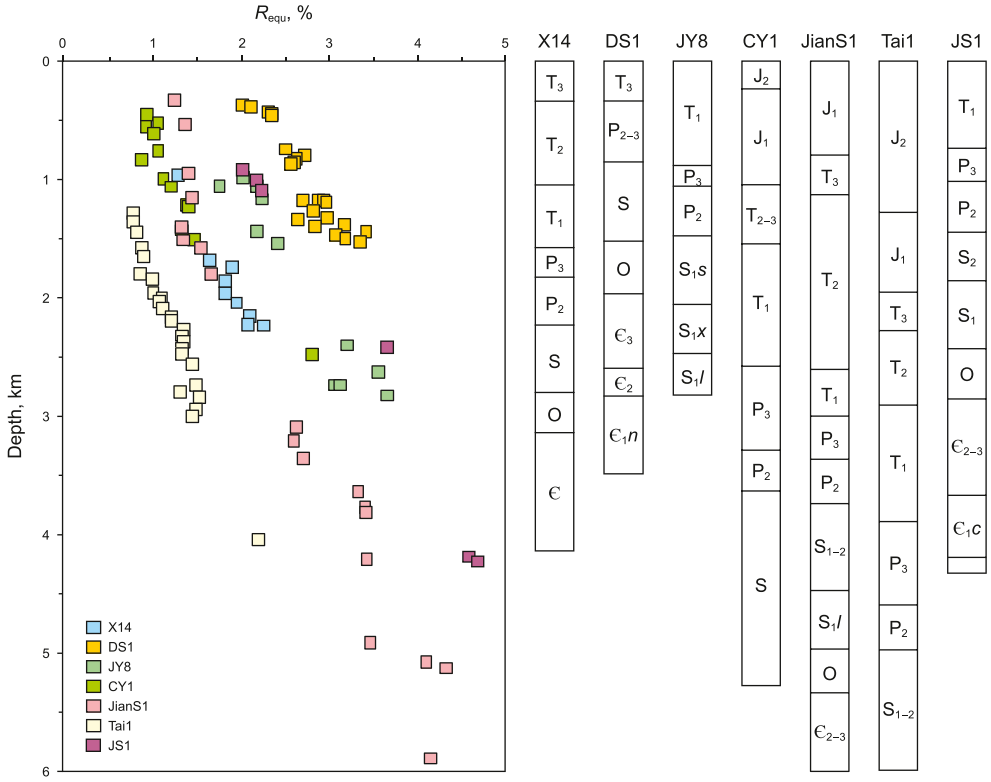

Fig. 7. The vitrinite reflectance data of typical wells in the eastern Sichuan Basin.

5.2. Thermal history of typical wells

Well T1 in the eastern Sichuan Basin penetrated the Permian basalt at a depth of 4762–4772.5 m. (Zhu et al., 2018; Fig. 9(a) and (b)). R_{equ} data near the basalt exhibit discontinuities, with the values in the Middle Permian Maokou Formation significantly exceeding those in the Upper Permian Longtan Formation and Middle Permian Qixia Formation (Fig. 9(b)). Previous studies attributed this anomaly to Permian high temperature (~150 °C) and elevated heat flow (110 mW/m^2) affecting Carboniferous and Middle Permian strata (Feng et al., 2022; Jiang et al., 2018; Zhu et al., 2010, 2018; Fig. 9(c)). While magmatic intrusion can thermally perturb adjacent strata, the thermal effect diminishes with distance from the intrusion (Duan et al., 2023; Jiang et al., 2021; Tang et al., 2013), typically extending up to twice the magmatic intrusion's thickness (Bulguroglu and Milkov, 2020; Feng et al., 2018). For T1's 10.5-m-thick basalt, this implies a maximum thermal effect of ~21 m, insufficient to impact the ~400 m-thick Qixia Formation (Fig. 9(a)). Low-temperature thermochronology indicates that Devonian strata beneath Carboniferous strata experienced temperatures of 100–120 °C during the Middle Permian (Fig. 8(i)), constraining Carboniferous and Middle Permian strata to lower than 100–120 °C. To reconcile discrepancies, anomalous R_{equ} data (highlighted in Fig. 9(b)) were

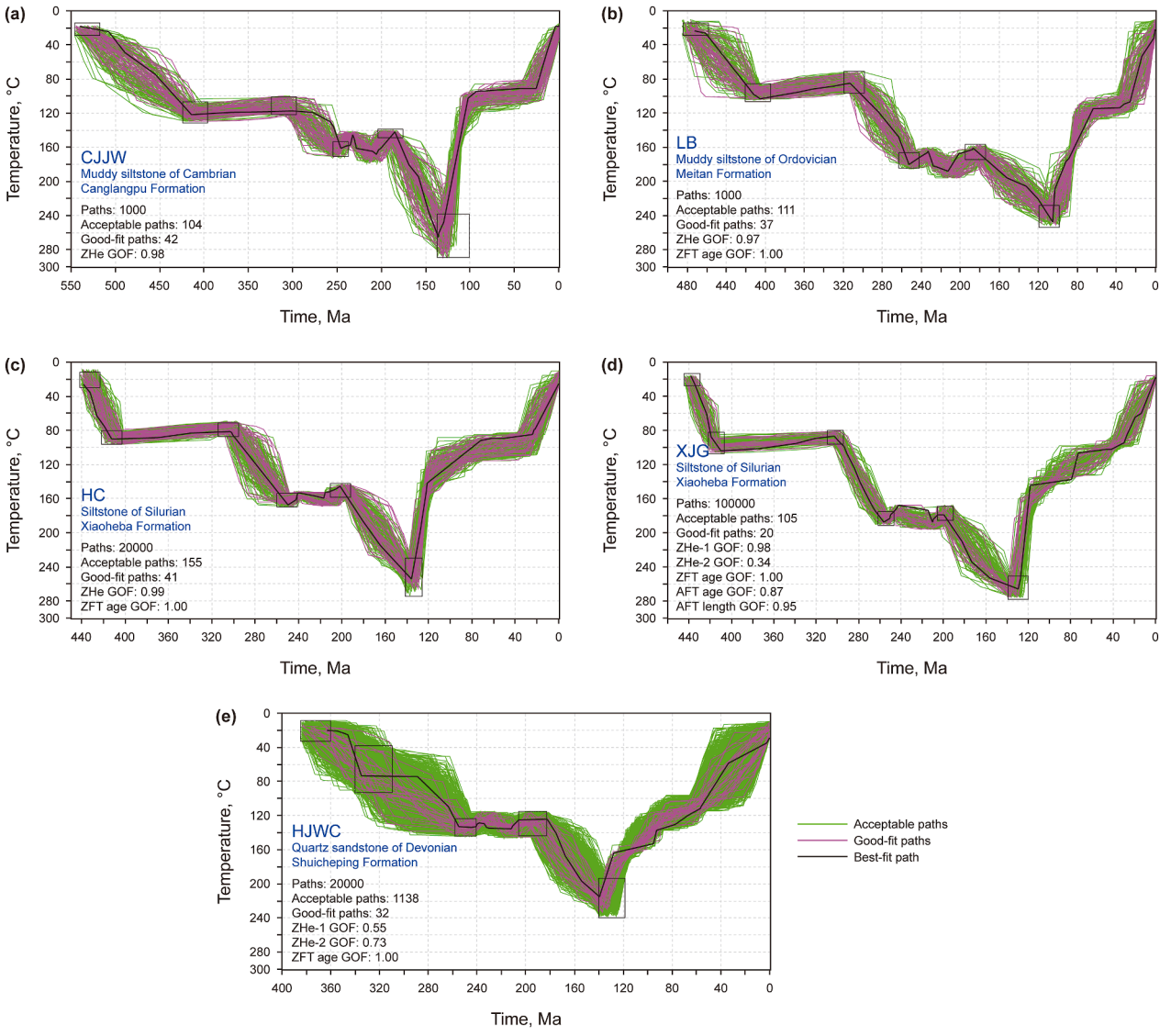

Fig. 8. Thermal modeling results of the nine outcrop clastic rock samples. Green lines, pink lines and black lines represent the acceptable fit paths (GOF >0.05), good fit paths (GOF >0.5), and the best path, respectively. GOF is the goodness of fit.

excluded, and simulation was rerun using the burial history (Fig. 9 (a)) and the EasyR_o% model. Revised result (Fig. 9(d)) yield Middle Permian temperatures of ~100 °C and peak heat flow of 65 mW/m^2 for these strata, aligning with thermal modeling (Fig. 8(i)). Post-correction, measured and simulated R_{equ} values exhibit markedly consistency (Fig. 9(e)), validating the revised thermal history.

Under the constraint of the thermal histories modeled by the ZFT and ZHe paleothermometer (Fig. 8), the burial and thermal evolution of the seven typical wells in the study area were reconstructed using BasinMod 1D software. The compaction and porosity exponential reducing factors (Sclater and Christie, 1980) and EasyR_o% model (Sweeney and Burnham, 1990) were chosen in the software. Results of the integrated burial-thermal histories are presented in Fig. 10. Notably, the simulated R_{equ} values demonstrate consistency with measured data.

The heat flow histories of the typical wells are shown in Fig. 11. From the Cambrian to the Carboniferous, the eastern Sichuan Basin was in a steady thermal state by low heat flow (45–55 mW/m^2). Then, the heat flow increased rapidly from the Early Permian to the Middle Permian, and the heat flow peaked in the Middle Permian with heat flow values of 62–70 mW/m^2. The heat flow declined precipitously in the Early-Middle Triassic because of thermal state of the Sichuan Basin is gradually stabilizing, and reached its current stable value of 47–62 mW/m^2.

5.3. Maturity evolution of the Paleozoic source rocks

The Qiongzhusi Formation source rocks initiated hydrocarbon generation (R_{equ} = 0.5%) during the Late Cambrian to Late Ordovician. Maturation progressed slowly thereafter because of tectonic events associated with the Caledonian and Indosinian movements. A pronounced increase in maturity occurred from the Late Permian to Early Triassic due to the peak heat flow, followed by sustained maturation during the Jurassic to Late Cretaceous owing to continuous deposition of strata. This protracted thermal evolution culminating in peak maturation (R_{equ} = 4%–4.5%.) during the Late Cretaceous. Subsequent intense uplift during the

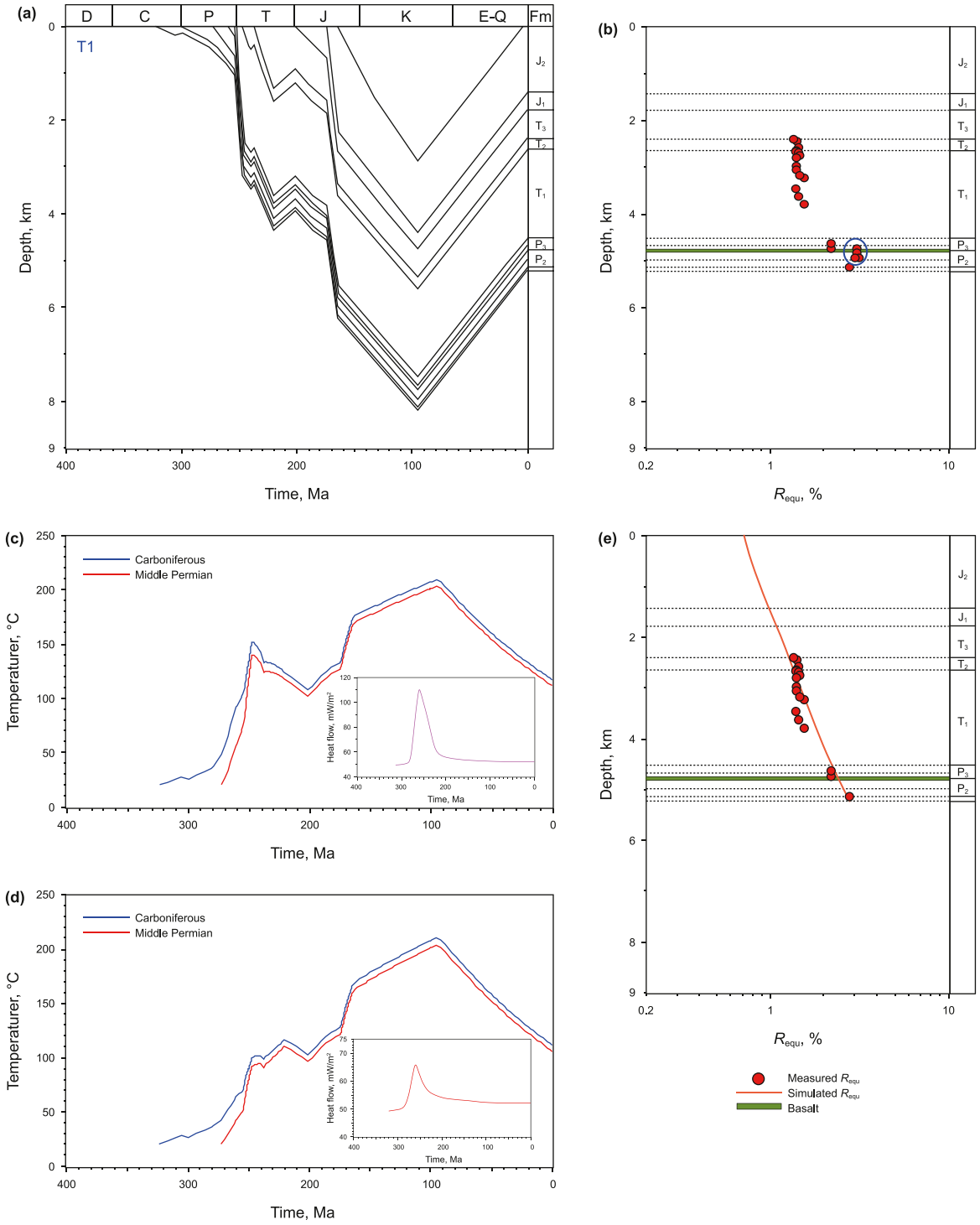

Fig. 9. (**a**) Burial history of Well T1. **(b)** Measured R_{equ} of Well T1. **(c)** The temperature histories of the Carboniferous and Middle Permian under abnormal high peak heat flow of 110 mW/m^2 in Well T1. **(d)** The temperature histories of the Carboniferous and Middle Permian under peak heat flow of 65 mW/m^2. **(e)** Simulated R_{equ} of Well T1, when eliminate abnormal R_{equ}.

Yanshan-Himalayan movement halted further maturation, leaving source rocks in an over-mature state at present (Fig. 12(a)).

The Longmaxi Formation source rocks attained early maturity in the Late Silurian to Early Devonian. Their maturation was subdued during the Caledonian and Indosinian orogenies, but accelerated markedly in the Late Permian – Early Triassic and Jurassic to Late Cretaceous. Peak maturity (R_{equ} = 3%–4%) was reached in the Late Cretaceous, followed by stagnation due to Yanshan-Himalayan tectonic activity, resulting in present-day over-maturity (Fig. 12(b)).

For Lower Permian source rocks, hydrocarbon generation commenced in the Late Permian, progressing to mid-maturity by the Early Triassic. Maturity stalled during the Indosinian orogeny but resumed rapidly with renewed subsidence until the Jurassic.

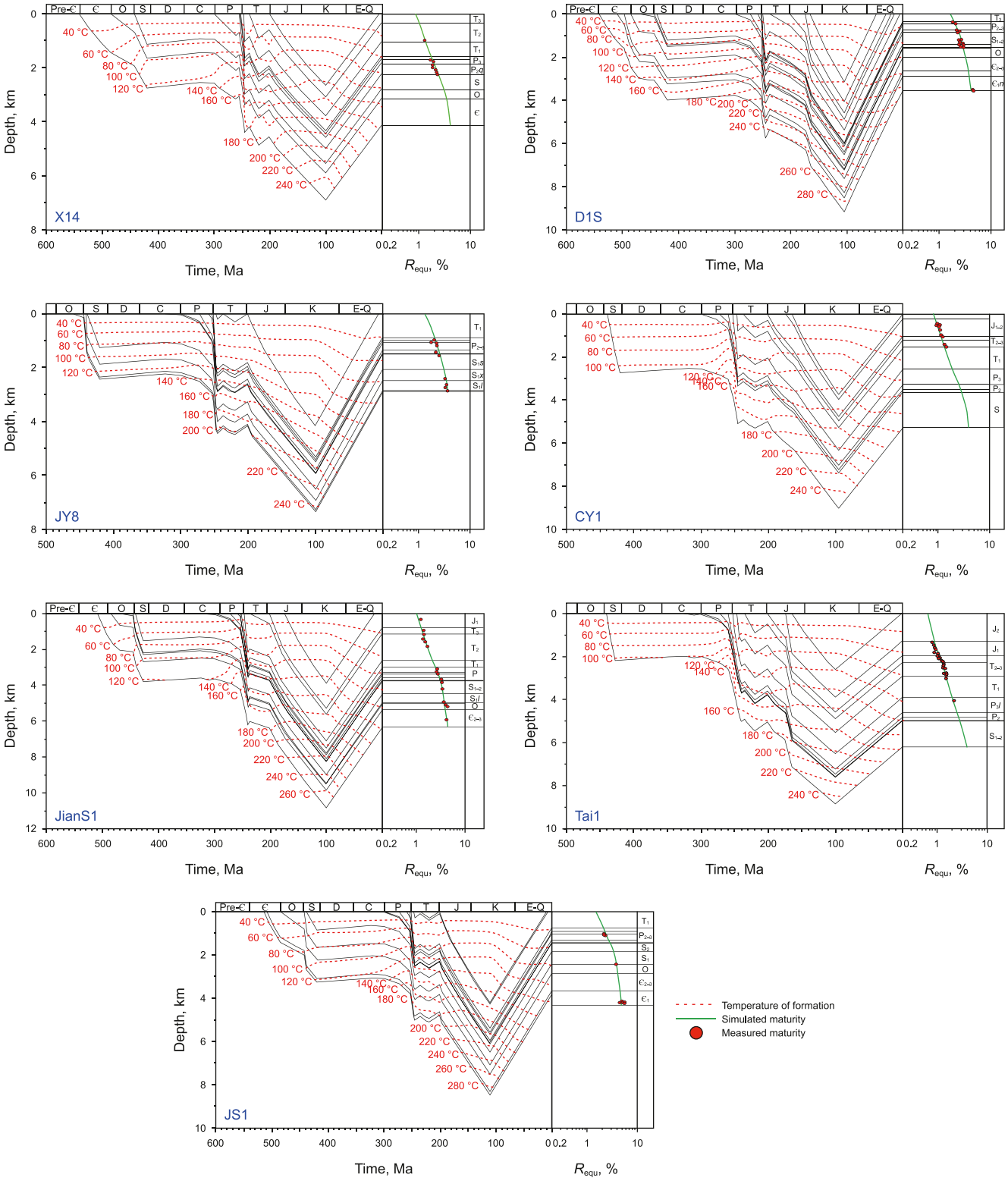

Fig. 10. The burial and thermal history of typical wells in the eastern Sichuan Basin.

Peak maturity (R_{equ} = 2.5%–3%) was achieved in the Late Cretaceous. However, widespread uplift and erosion linked to the Yanshan-Himalayan orogeny terminated further maturation (Fig. 12(c)). The Upper Permian Longtan Formation source rocks reached early maturity in the Early Triassic, following a maturation trajectory similar to the Lower Permian source rocks. The peak maturity was about 2%–3% in the Late Cretaceous (Fig. 12 (d)).

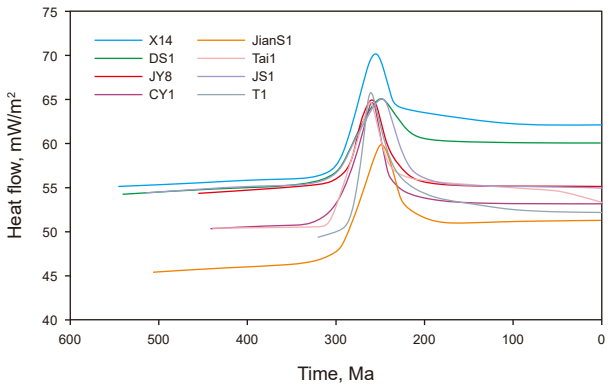

Fig. 11. The heat flow history in the eastern Sichuan Basin.

6. Discussion

6.1. Contributing factor to Permian abnormal heat flow in the eastern Sichuan Basin

Tectonic evolution indicates that the Yangtze Block underwent the EMP and lithospheric extension during the Permian (Li et al., 2017; Liu et al., 2022; Wang et al., 2024; Xiao et al., 2023). This study constrains the Permian abnormal heat flow in eastern Sichuan Basin to 62–70 mW/m^2, representing a 15–17 mW/m^2 increase above the stable Paleozoic heat flow values (45–55 mW/m^2) (Figs. 11 and 13). Notably, no evidence supports localized heat flow exceeding 100 mW/m^2 in the study area. In contrast, the western and central Sichuan Basin experienced significantly higher Permian abnormal heat flow of 75–114 mW/m^2 (Fig. 13), exceeding Paleozoic values (50–60 mW/m^2) by 20–64 mW/m^2 (Feng et al., 2021, 2022; Qiu et al., 2022; Zhu et al., 2010). Geodynamic simulations using a multiple episode stretching model suggest lithospheric extension during rifting could elevate heat flow by ~20% initial values in the basins (He et al., 2011).

In the eastern Sichuan Basin, Middle-Late Permian lithospheric extension associated with the Kaijiang-Liangping trough (Fig. 1(b)) generated syn-rift magmatism, evidenced by basalts interbedded Maokou Formation limestone, volcanic carbonates, and mud-rich breccias. These basalts were emplaced prior to EMP activity (Deng et al., 2024), and records hydrothermal activities and thermal anomalies linked to trough formation. Numerical simulations confirm that EMP-derived material did not reach the eastern Sichuan Basin, and the Permian basalts in the eastern Sichuan Basin are distinct from the EMP (He, 2022). Thus, the Permian abnormal heat flow in eastern Sichuan Basin likely originated from lithospheric extension during the Kaijiang-Liangping trough development.

However, the western and central Sichuan Basin's higher Permian abnormal heat flow necessitate EMP involvement. This study infers an EMP's thermal effect radius of 600–650 km, consistent with estimates by He (2022).

6.2. Thermal effects of the EMP on the maturity evolution of Paleozoic source rocks in the Sichuan Basin

Mantle plumes, characterized by narrow, buoyant upwellings of high-temperature material with hundred(s)-kilometer scale from thermal boundary layers (Koppers et al., 2021), exert thermal effects through three primary mechanisms: (1) Ascending plume heads transfer heat from the deep mantle to the lithosphere, generating surface heat flow anomalies (He, 2022; Wang and Li, 2021). (2) High-temperature magmas exploit crustal faults to

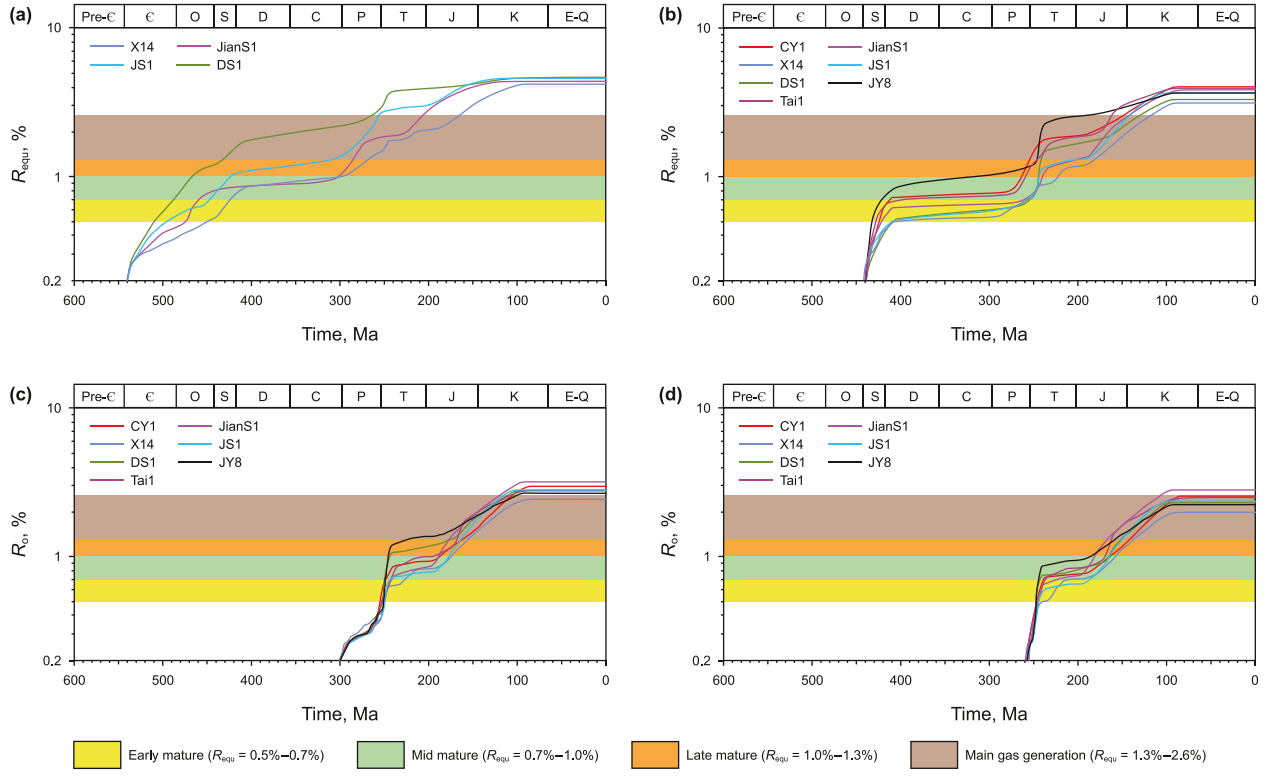

Fig. 12. (**a**) The maturity evolution of the Lower Cambrian Qiongzhusi Formation source rocks in the eastern Sichuan Basin. **(b)** The maturity evolution of the Lower Silurian Longmaxi Formation source rocks in the eastern Sichuan Basin. **(c)** The maturity evolution of the Lower Permian source rocks in the eastern Sichuan Basin. **(d)** The maturity evolution of the Upper Permian Longtan Formation source rocks in the eastern Sichuan Basin.

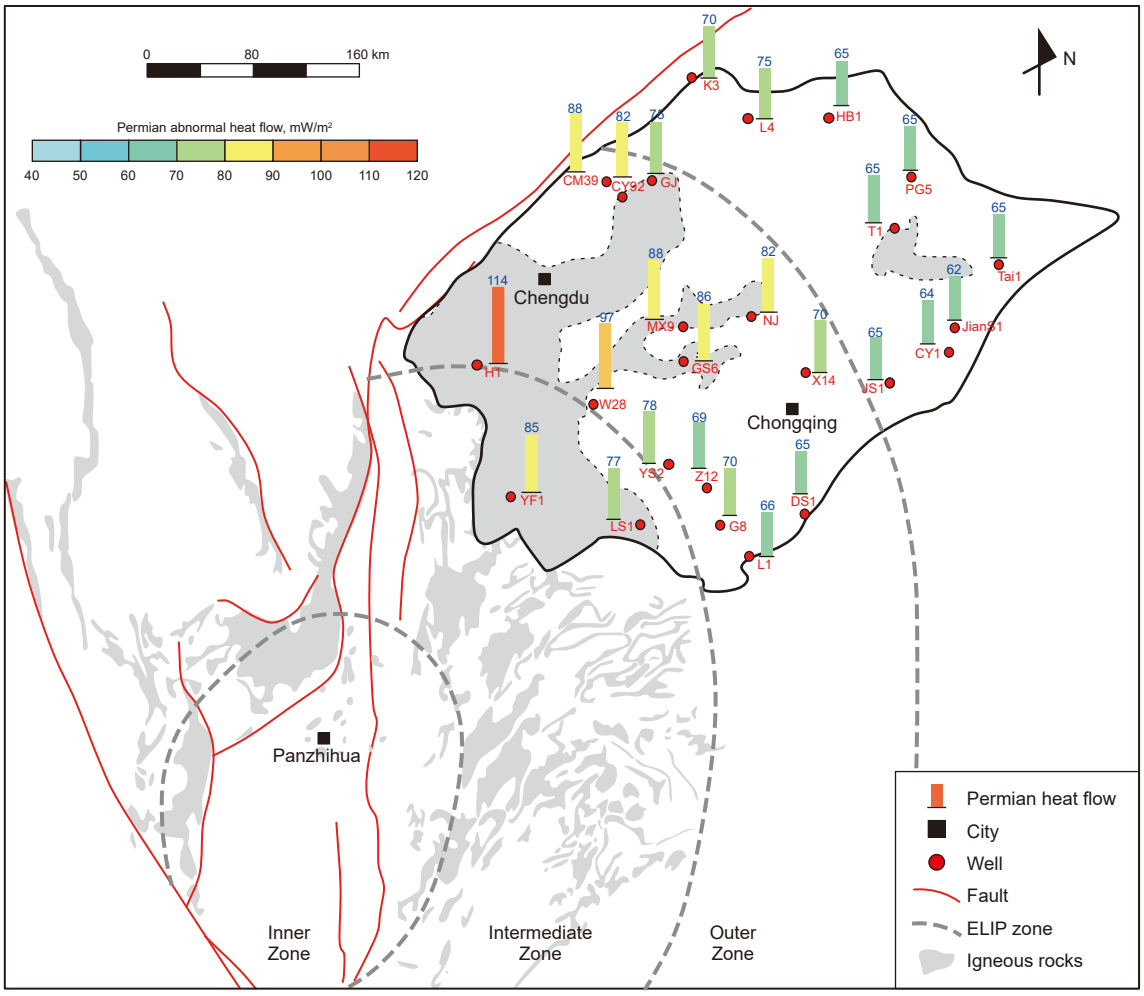

Fig. 13. The distribution of Permian abnormal heat flow in the Sichuan Basin and the thermal effect range of EMP (modified after Feng et al. (2021)).

intrude and thermally alter surrounding rocks (Jiang et al., 2021; Tang et al., 2013). (3) Rapid eruptions (<1 Ma) of mantle-derived mafic-ultramafic lavas induce transient of underlying strata (He et al., 2011; Hu et al., 2020; Zhu et al., 2010).

Numerical simulations indicate that the EMP dominantly affected the lithosphere above its plume head (inner and intermediate zones), with heat flow decreasing radially from >100 mW/m^2 in the inner zone to lower values outward (He et al., 2011; He, 2022). In the western Sichuan Basin, 300-m-thick EMP-derived lava flows increased temperatures in underlying Permian strata by > 100 °C within a 600 m vertical range (Wu et al., 2023b). Low-temperature thermochronology further reveals that Cambrian strata (~3000 m depth) experienced >200 °C heating when overlain by > 1500 m lavas (Hu et al., 2020). Notably, no geophysical or drilling evidence supports large-scale magmatic intrusions in the Sichuan Basin linked to the EMP, restricting its thermal effects to mechanisms (1) and (3).

The western and central Sichuan Basin, situated within the EMP's intermediate to outer zones (Fig. 1(b)), experienced Permian peak heat flows of 75–114 mW/m^2 by the first mechanism (Fig. 13) (Feng et al., 2021; Qiu et al., 2021, 2022). This thermal effect drove rapid maturation of deeply buried Cambrian Qiongzhusi Formation and Silurian Longmaxi Formation source rocks, with R_{equ} increased by 0.5%–1.5% for Cambrian (e.g., Wells YF1, W28, GS6) and 0.3% for Silurian (e.g., Well YF1) over ~ 1–2 Ma (Fig. 14). In areas with thick EMP lavas (~300 m) (Fig. 1(b)) (Liu et al., 2022; Ma et al., 2019), Lower Permian source rocks (e.g., Wells H1, YT1) matured rapidly from immature to over-mature (R_{equ} > 2.6%) at ~ 260 Ma (Fig. 14). Conversely, regions with thinner lavas (<80 m; e.g., Wells W28, GS6) (Fig. 1(b)) show no rapid maturation at ~ 260 Ma (Fig. 14), as insufficient lava thickness limited conductive heating (Bulguroglu and Milkov, 2020; Feng et al., 2018).

Located beyond the EMP's outer zone, the eastern Sichuan Basin exhibited low Permian heat flows (62–70 mW/m^2) and minimal thermal influence (Fig. 13). Sparse, thin basalts (20–65 m) in the eastern Sichuan Basin (Fig. 1(b)) (Liu et al., 2022; Ma et al., 2019) generated localized heating <50–80 m (Wu et al., 2023b), insufficient to affect the >300-m-thick Permian strata (Fig. 9). Consequently, Paleozoic strata show no thermal anomalies (Fig. 8) and source rocks matured gradually (Fig. 14), while Upper Permian Longtan Formation maturity remained unaffected due to its younger depositional age (Fig. 14).

In summary, the EMP's thermal effects exhibited distinct spatial zonation across the Sichuan Basin. In the western Sichuan Basin, rapid maturation of source rocks was driven by combined the first and third mechanism. The central Sichuan Basin experienced predominantly thermal effect driven by the first mechanism, while the EMP did not affect the eastern Sichuan Basin. These results align with the inferred EMP's thermal effect radius of 600–650 km.

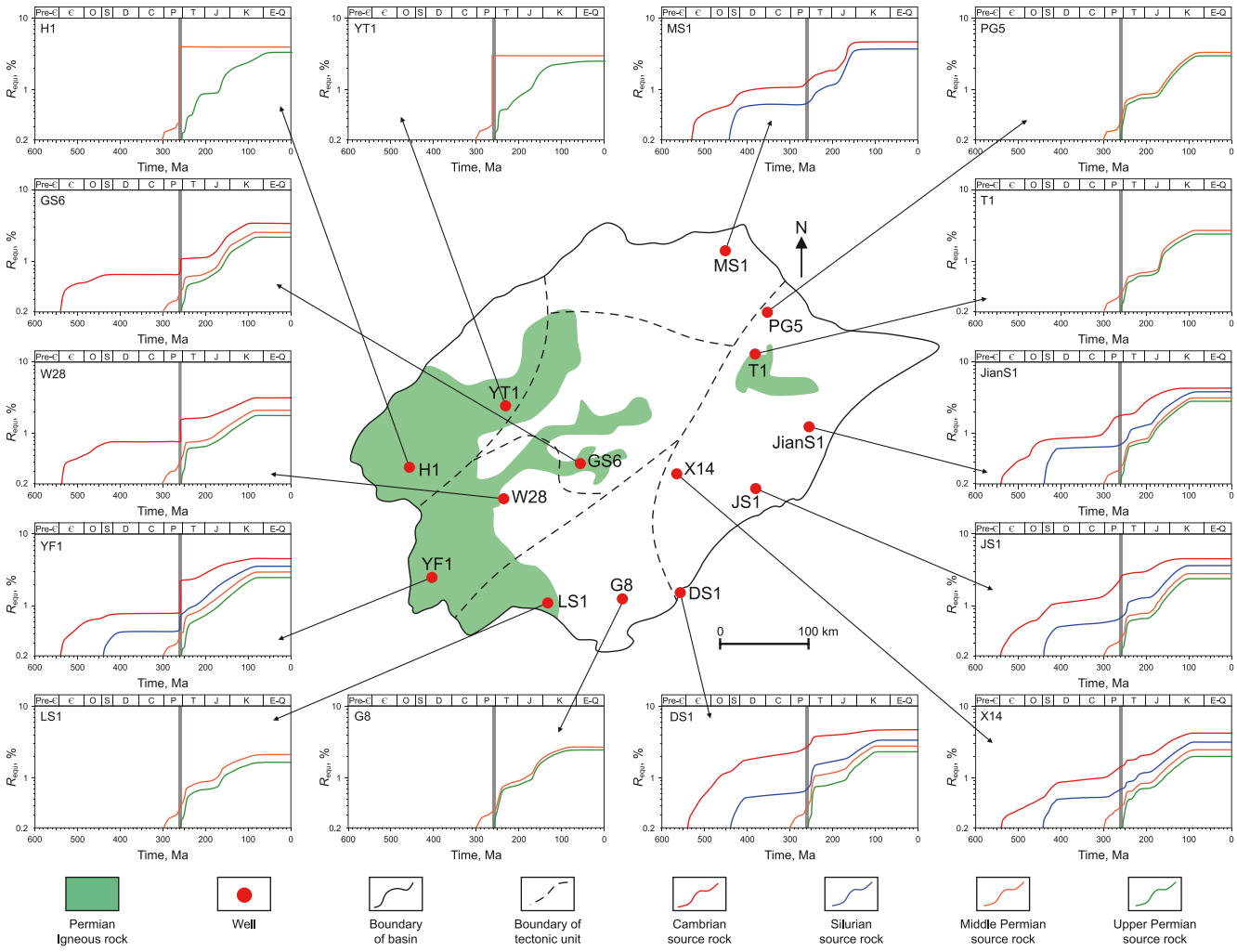

Fig. 14. The thermal evolution of Paleozoic source rocks in Sichuan Basin (Well GS6, MS1M W28, YF1, H1, YT1, LS1, and G8 cited from Feng et al., 2021, 2022; Qiu et al., 2022).

6.3. Geodynamic model of the Permian thermal regime in the eastern Sichuan Basin

Previous study suggests that the Kaijiang-Liangping trough initiated during the Middle Permian Qixia Stage, expanded through the Maokou Stage, gradually subsided after the Maokou Stage, and closed by the Middle Triassic (Deng et al., 2021). This evolutionary timeline aligns with the Early Permian– Middle Triassic heat flow trends in the eastern Sichuan Basin. Building on this framework, we present a geodynamic model to explain the Permian thermal regime (Fig. 15).

In the Middle Permian Qixia Stage, transient asthenospheric upwelling collided with the lithosphere beneath the eastern Sichuan Basin carbonate platform. Limited lithospheric extension prevented magma ascent to the surface (Fig. 15(a)). During the Early Maokou Stage (~272 Ma), lithospheric extension remained relatively subdued, facilitating the deposition of carbonate strata with several hundred meters thick. Until the Middle Maokou Stage (~267 Ma), both lithospheric extension and asthenospheric magmatic upwelling intensified (Deng et al., 2021). This enhanced magmatic upwelling activated the Huayinshan Fault in the eastern Sichuan Basin, allowing transient small-scale magma ascent to the Middle Permian Maokou Formation. Associated thermal perturbations generated a peak heat flow of 62–70 mW/m^2 (Fig. 15(b)), reflecting syn-rift magmatism preceding the main phase of EMP activity.

During the Middle Permian, the upwelling of the EMP beneath the southwestern of the Yangtze Block triggered crustal uplift, formation of the Kangdian paleohigh, and intense erosion of the Maokou Formation. Concurrent lithospheric extension and thinning activated multiple basement faults. As the mantle plume continuously collided with the lithosphere, its head expanded northeastward by 600–650 km, terminating near the central Sichuan Basin. By the Late Maokou Stage (~260Ma), high-temperature magmas intruded and erupted along these faults, producing lava flows from several kilometers to dozens of meters in thickness across the inner to outer zones (Fig. 15(c)). This mantle plume activity generated peak heat flow values of 75–114 mW/m^2, driving rapid maturation of Paleozoic source rocks and mass high-temperature methane release in the western and central Sichuan Basin (Feng et al., 2025). In contrast, lavas in the eastern Sichuan Basin, far from the inner zone, underwent rapid solidification within a few million years.

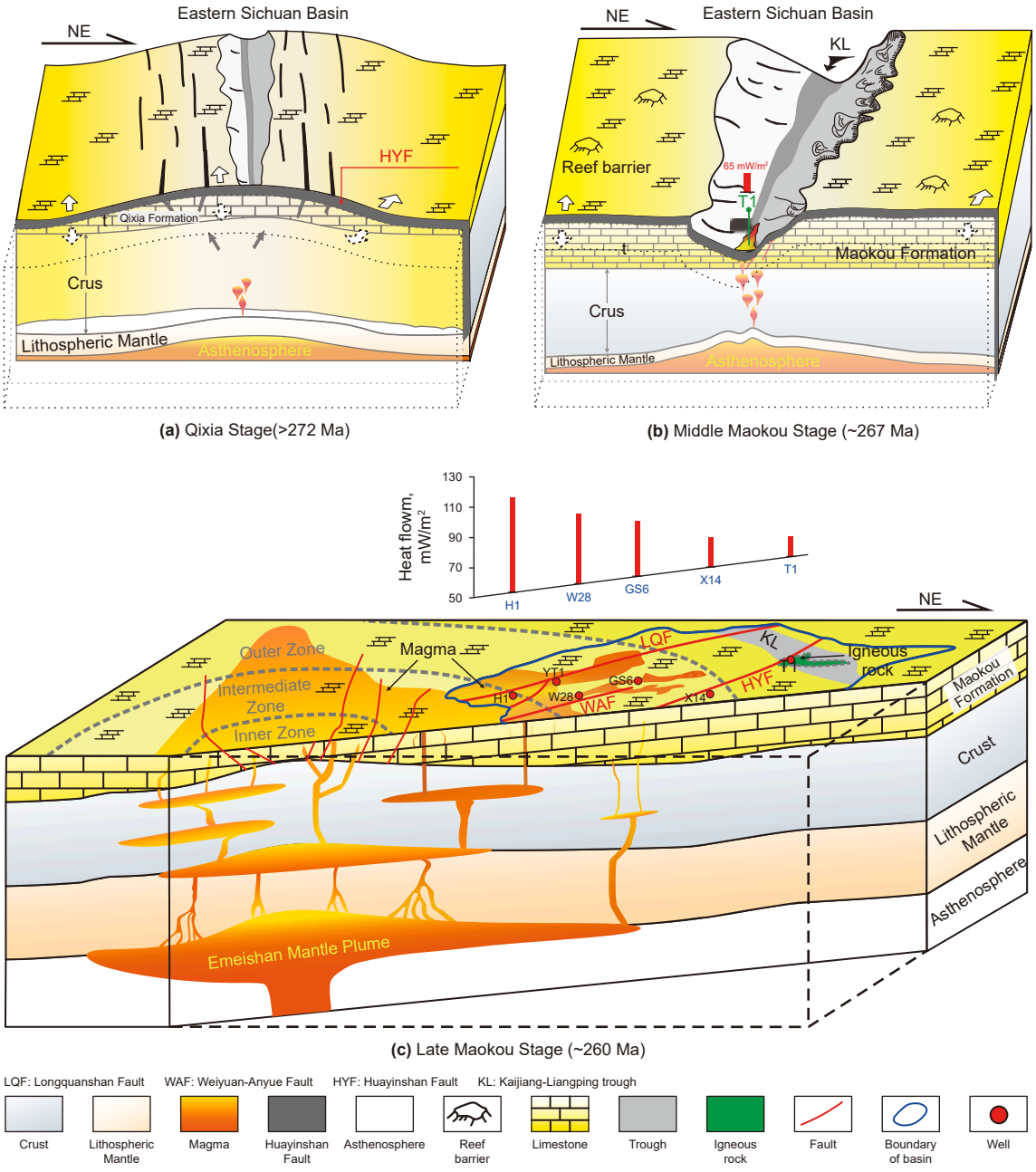

Fig. 15. The geodynamic model of Permian thermal regime in the Sichuan Basin ((**a**) and (**b**) are modified from Deng et al., 2024.

7. Conclusions

(1) The heat flow evolution in the eastern Sichuan Basin since the Paleozoic is characterized by three distinct stages: the stable low heat flow stage from the Cambrian to Permian, with heat flow values ranging from 45 to 55 mW/m^2; the heat flow escalation stage in the Permian, reaching peak values of 62–70 mW/m^2; the heat flow attenuation and stabilization stage from the Triassic to present day, during which heat flow returned to 47–62 mW/m^2.

(2) The thermal evolution of Paleozoic source rocks in the eastern Sichuan Basin is tectonically controlled. Multi-phase tectonic movements (Caledonian, Indosinian, and Yanshan-Himalayan orogenies) caused multi periods maturation stagnation, while peak heat flow in the Permian and rapid burial in the Jurassic–Late Cretaceous accelerated maturation. Generating hydrocarbons (R_{equ}=0.5%) in the Late Cambrian–Late Ordovician for the Cambrian Qiongzhusi Formation source rock, followed by the Late Silurian–Early Devonian for the Silurian Longmaxi Formation source rock, while Late Permian–Early Triassic for the Permian source rocks. These source rocks reached peak maturity (4%–4.5% for the Qiongzhusi Formation source rock, 3%–4% for the Longmaxi Formation source rock, 2%–3% for the Permian source rocks) in the Late Cretaceous. Present-day overmaturity dominates across these source rocks.

(3) The EMP's thermal effect significantly influenced the western and central Sichuan Basin, with rapidly maturation of Paleozoic source rocks. The radius of the thermal effect is estimated at ~600–650 km. However, the eastern Sichuan

Basin's Permian thermal regime was governed by lithospheric extension during the Middle Permian Kaijiang-Liangping trough rifting, independent of EMP's thermal effect.

CRediT authorship contribution statement

Xin Liu: Writing – review & editing, Writing – original draft, Visualization, Validation, Methodology, Investigation, Formal analysis, Data curation, Conceptualization. **Nan-Sheng Qiu:** Writing – review & editing, Resources, Project administration, Funding acquisition. **Qian-Qian Feng:** Writing – review & editing, Supervision, Resources, Project administration, Methodology, Funding acquisition, Conceptualization.

Declaration of competing interest

The authors declare that they have no known competing financial interests or personal relationships that could have appeared to influence the work reported in this paper.

Acknowledgments

This work was supported by The National Natural Science Foundation of China [U2244208,42302138]; and the Science Foundation of China University of Petroleum, Beijing [2462024XKQY001]. Thanks Professor Chang Jian for the suggestions in the writing of the manuscript. Thanks to the editor and reviewers for their detail comments that helped to improve the manuscript.

References

Bulguroglu, M.E., Milkov, A.V., 2020. Thickness matters: Influence of dolerite sills on the thermal maturity of surrounding rocks in a coal bed methane play in Botswana. Mar. Petrol. Geol. 111, 219–229. https://doi.org/10.1016/j.marpetgeo.2019.08.016.

Cai, C.E., Qiu, N.S., Li, H.L., et al., 2020. Study of the closure temperature of (U-Th)/He in detrital zircon obtained from natural evolution samples. Sci. China Earth Sci. 50 (1), 66–78. (in Chinese). https://doi.org/10.1360/SSTe-2019-0066.

Cao, H.Y., Zhu, C.Q., Qiu, N.S., 2015. Thermal evolution of Lower Silurian longmaxi formation in the eastern Sichuan Basin. J. Earth Sci. Environ. 37 (6), 22–32 (in Chinese).

Chen, J.P., Li, W., Ni, Y.Y., et al., 2018a. The Permian source rocks in the Sichuan basin and its natural gas exploration potential (Part 1): spatial distribution of source rocks. Nat. Gas. Ind. 38 (5), 1–16. https://doi.org/10.3787/j.issn.1000-0976.2018.05.001.

Chen, J.P., Li, W., Ni, Y.Y., et al., 2018b. The Permian source rocks in the Sichuan basin and its natural gas exploration potential (Part 2): geochemical characteristics of source rocks and latent capacity of natural gas resources. Nat. Gas. Ind. 38 (6), 33–45. (in Chinese). https://doi.org/10.3787/j.issn.1000-0976.2018.06.005.

Chen, M.J., Tan, K.J., Wen, L., et al., 2023. Natural gas accumulation characteristics and great exploration potential of the Middle Permian in the Sichuan Basin. Earth Sci. Front. 30 (1), 11–19. (in Chinese). https://doi.org/10.13745/j.esf.sf.2022.8.23.

Cheng, C., Li, S., Xie, X., et al., 2022. Sedimentary evolution and sea-level fluctuation of a Paleo-Tethyan Permian carbonate-dominated succession from central China. Sediment. Geol. 440, 106244. https://doi.org/10.1016/j.sedgeo.2022.106244.

Dai, J.X., Ni, Y.Y., Liu, Q.Y., et al., 2021. Sichuan super gas basin in southwest China. Petrol. Explor. Dev. 48 (6), 1251–1259. https://doi.org/10.1016/S1876-3804(21)60284-7.

Deng, L., Yang, J., Yan, Q., et al., 2024. Rifting of the upper Yangtze carbonate platform: Insight from Middle Permian carbonate olistostromes in the NE Sichuan Basin, SW China. J. Asian Earth Sci. 260, 105973. https://doi.org/10.1016/j.jseaes.2023.105973.

Deng, L., Yan, Q.R., Song, B., et al., 2021. Sedimentary responses to rifting of the Upper Yangtze block (Sichuan Basin area) in the middle-Late Permian. Acta Petrol. Sin. 37 (8), 2465–2482. (in Chinese). https://doi.org/10.18654/1000-0569/2021.08.13.

Dong, Y., Sun, S., Santosh, M., et al., 2021. Central China orogenic belt and amalgamation of East Asian continents. Gondwana Res. 100, 131–194. https://doi.org/10.1016/j.gr.2021.03.006.

Duan, W., Shi, L., Luo, C.F., et al., 2023. Response of clastic reservoir to magmatic intrusion: Advances and prospects. Geoenergy Sci. Eng. 227, 211938. https://doi.org/10.1016/j.geoen.2023.211938.

Feng, L., Zeng, H.S., Wang, H.W., 2018. Impact of igneous intrusion on the thermal evolution of source rocks with different maturities: A case study of Fangzheng Fault Depression and Suibin Sag in north-eastern China. Petrol. Geol. Exp. 40 (5), 724–729. (in Chinese). https://doi.org/10.11781/sysydz201805724.

Feng, Q., Qiu, N., Fu, X., et al., 2022. Maturity evolution of Permian source rocks in the Sichuan Basin, southwestern China: The role of the Emeishan mantle plume. J. Asian Earth Sci. 229, 105180. https://doi.org/10.1016/j.jseaes.2022.105180.

Feng, Q., Qiu, N., Fu, X., et al., 2021. Permian geothermal units in the Sichuan Basin: Implications for the thermal effect of the Emeishan mantle plume. Mar. Petrol. Geol. 132, 105226. https://doi.org/10.1016/j.marpetgeo.2021.105226.

Feng, Q., Qiu, N., Wu, H., et al., 2023. Thermo-kinematic constraints on restoration of the eastern Sichuan fold-and-thrust Belt, South China. Tectonics 42, e2022TC007630. https://doi.org/10.1029/2022TC007630.

Feng, Q., Qiu, N., Fu, X., et al., 2025. Permian thermal pulse event in Southwestern China and its resource and environment effects. Global Planet. Change 246, 104722. https://doi.org/10.1016/j.gloplacha.2025.104722.

Flowers, R.M., Ketcham, R.A., Shuster, D.L., et al., 2009. Apatite (U-Th)/He thermochronometry using a radiation damage accumulation and annealing model. Geochem. Cosmochim. Acta 73 (8), 2347–2365. https://doi.org/10.1016/j.gca.2009.01.015.

Flowers, R.M., Shuster, D.L., Wernicke, B.P., et al., 2007. Radiation damage control on apatite (U-Th)/He dates from the Grand Canyon region, Colorado Plateau. Geology (Boulder) 35 (5), 447–450. https://doi.org/10.1130/G23471A.1.

Gautheron, C., Barbarand, J., Ketcham, R.A., et al., 2013. Chemical influence on α-recoil damage annealing in apatite: Implications for (U-Th)/He dating. Chem. Geol. 351, 257–267. https://doi.org/10.1016/j.chemgeo.2013.05.027.

Gautheron, C., Tassan-Got, L., 2010. A Monte Carlo approach to diffusion applied to noble gas/helium thermochronology. Chem. Geol. 273 (3–4), 212–224. https://doi.org/10.1016/j.chemgeo.2010.02.023.

Guenthner, W.R., Reiners, P.W., Ketcham, R.A., et al., 2013. Helium diffusion in natural zircon: radiation damage, anisotropy, and the interpretation of zircon (U-Th)/He thermochronology. Am. J. Sci. 313 (3), 145–198. https://doi.org/10.1016/j.gca.2020.01.049.

He, B., Xu, Y.G., Wang, Y.M., et al., 2006. Sedimentation and lithofacies paleogeography in Southwestern China before and after the emeishan flood volcanism: New insights into surface response to mantle plume activity. J. Geol. 114 (1), 117–132. https://doi.org/10.1086/498103.

He, L., 2022. Emeishan mantle plume and its potential impact on the Sichuan Basin: Insights from numerical modeling. Phys. Earth Planet. Inter. 323, 106841. https://doi.org/10.1016/j.pepi.2022.106841.

He, L.J., Xu, H.H., Wang, J.Y., 2011. Thermal evolution and dynamic mechanism of the Sichuan Basin during the early Permian-middle Triassic. Sci. China Earth Sci. 54, 1948–1954. https://doi.org/10.1007/s11430-011-4240-z.

Hong, H.T., Tian, X.W., Sun, Y.T., et al., 2020. Hydrocarbon enrichment regularity of marine carbonate in Sichuan Basin. Geol. China 47 (1), 99–110. (in Chinese). https://doi.org/10.12029/gc20200108.

Hu, D., Tian, Y., Hu, J., et al., 2020. Thermal imprints of late Permian Emeishan basalt effusion: Evidence from zircon fission-track thermochronology. Lithos 352–353, 105224. https://doi.org/10.1016/j.lithos.2019.105224.

Hu, J., Yang, H., Badal, J., et al., 2023. Decoding the Emeishan Permian mantle plume in the southeastern margin of Tibet from the seismic signature of the local lithosphere. Geophys. J. Int. 232 (1), 81–96. https://doi.org/10.1093/gji/ggac327.

Huang, H., Huyskens, M.H., Yin, Q., et al., 2022. Eruptive tempo of Emeishan large igneous province, southwestern China and northern Vietnam: Relations to biotic crises and paleoclimate changes around the Guadalupian-Lopingian boundary. Geology 50 (9), 1083–1087. https://doi.org/10.1130/G50183.1.

Jiang, G., Hu, S., Shi, Y., et al., 2019. Terrestrial heat flow of continental China: updated dataset and tectonic implications. Tectonophysics 753, 36–48. https://doi.org/10.1016/j.tecto.2019.01.006.

Jiang, J., Zhao, K., Cheng, Y., et al., 2021. Numerical simulation of magma intrusion on the thermal evolution of low-rank coal. Environ. Earth Sci. 80, 562. https://doi.org/10.1007/s12665-021-09871-5.

Jiang, Q., Jourdan, F., Olierook, H.K.H., et al., 2023a. An appraisal of the ages of Phanerozoic large igneous provinces. Earth Sci. Rev. 237, 104314. https://doi.org/10.1016/j.earscirev.2023.104314.

Jiang, P.F., Wu, J.F., Zhu, Y.Q., et al., 2023b. Enrichment conditions and favorable areas for exploration and development of marine shale gas in Sichuan Basin. Acta Petrol. Sin. 44 (1), 91–109. (in Chinese). https://doi.org/10.7623/syxb202301006.

Jiang, Q., Qiu, N., Zhu, C., 2018. Heat flow study of the Emeishan large igneous province region: implications for the geodynamics of the Emeishan mantle plume. Tectonophysics 724–725, 11–27. https://doi.org/10.1016/j.tecto.2017.12.027.

Ketcham, R.A., Carter, A., Donelick, R.A., et al., 2007. Improved modeling of fission-track annealing in apatite. Am. Mineral. 92 (5–6), 799–810. https://doi.org/10.2138/am.2007.2281.

Ketcham, R.A., Gautheron, C., Tassan-Got, L., 2011. Accounting for long alpha-particle stopping distances in (U-Th-Sm)/He geochronology: Refinement of the baseline case. Geochem. Cosmochim. Acta 75 (24), 7779–7791. https://doi.org/10.1016/j.gca.2011.10.011.

Koppers, A.A.P., Becker, T.W., Jackson, M.G., et al., 2021. Mantle plumes and their role in Earth processes. Nat. Rev. Earth Environ. 2 (6), 382–401. https://doi.org/10.1038/s43017-021-00168-6.

Li, H., Zhang, Z., Santosh, M., et al., 2017. Late Permian basalts in the Yanghe area, eastern Sichuan Province, SW China: Implications for the geodynamics of the Emeishan flood basalt province and Permian global mass extinction. J. Asian Earth Sci. 134, 293–308. https://doi.org/10.1016/j.jseaes.2016.11.029.

Li, J.Z., Gu, Z.D., Lu, W.H., et al., 2021. Main factors controlling the formation of giant marine carbonate gas fields in the Sichuan Basin and exploration ideas. Nat. Gas. Ind. 41 (6), 13–26. (in Chinese). https://doi.org/10.3787/j.issn.1000-0976.2021.06.002.

Li, Y., Ding, W., Zeng, T., et al., 2023. Structural geometry and kinematics of a strike-slip fault zone in an intracontinental thrust system: A case study of the no. 15 fault zone in the Fuling area, eastern Sichuan Basin, southwest China. J. Asian Earth Sci. 242, 105512. https://doi.org/10.1016/j.jseaes.2022.105512.

Liu, G.X., Jin, Z.J., Deng, M., et al., 2015. Exploration potential for shale gas in the Upper Permian Longtan Formation in eastern Sichuan Basin. Oil Gas Geol. 36 (3), 481–487. (in Chinese). https://doi.org/10.11743/ogg20150317.

Liu, S., Yang, Y., Deng, B., et al., 2021a. Tectonic evolution of the Sichuan Basin, Southwest China. Earth Sci. Rev. 213, 103470. https://doi.org/10.1016/j.earscirev.2020.103470.

Liu, W., Qiu, N.S., Xu, Q.C., et al., 2018. Precambrian temperature and pressure system of Gaoshiti-Moxi block in the central paleo-uplift of Sichuan Basin, southwest China. Precambr. Res. 313, 91–108. https://doi.org/10.1016/j.precamres.2018.05.028.

Liu, X., Qiu, N., Søager, N., et al., 2022. Geochemistry of late Permian basalts from boreholes in the Sichuan Basin, SW China: Implications for an extension of the Emeishan large igneous province. Chem. Geol. 588, 120636. https://doi.org/10.1016/j.chemgeo.2021.120636.

Liu, X., Qiu, N.S., Feng, Q.Q., et al., 2023. Thermal evolution of the Permian in the eastern Sichuan Basin under the constraint of carbonate clumped isotopes. Acta Geol. Sin. 97 (8), 2676–2689. (in Chinese). https://doi.org/10.19762/j.cnki.dizhixuebao.2023250.

Liu, X., Qiu, N., Feng, Q., 2024. The thermal history of Permian carbonate strata reconstructed with clumped isotopes and U-Pb dating: Eastern Sichuan Basin, SW China. Mar. Petrol. Geol. 163, 106767. https://doi.org/10.1016/j.marpetgeo.2024.106767.

Liu, Y., Li, L., van Wijk, J., et al., 2021b. Surface-wave tomography of the Emeishan large igneous province (China): Magma storage system, hidden hotspot track, and its impact on the Capitanian mass extinction. Geology 49 (9), 1032–1037. https://doi.org/10.1130/G49055.1.

Luo, Q., Xiao, Z., Dong, C., et al., 2019. The geochemical characteristics and gas potential of the Longtan Formation in the eastern Sichuan Basin, China. J. Petrol. Sci. Eng. 179, 1102–1113. https://doi.org/10.1016/j.petrol.2019.04.101.

Ma, X.H., Li, G.H., Ying, D.L., et al., 2019. Distribution and gas-bearing properties of Permian igneous rocks in Sichuan Basin, SW China. Petrol. Explor. Dev. 46 (2), 228–237. https://doi.org/10.1016/S1876-3804(19)60004-2.

Meng, F., Tian, Y., Kerr, A.C., et al., 2023. Geochemistry and petrogenesis of late Permian basalts from the Sichuan Basin, SW China: Implications for the geodynamics of the Emeishan mantle plume. J. Asian Earth Sci. 241, 105477. https://doi.org/10.1016/j.jseaes.2022.105477.

Paton, C., Hellstrom, J., Paul, B., et al., 2011. Iolite: Freeware for the visualisation and processing of mass spectrometric data. J. Anal. Atomic Spectrom. 26 (12), 2508. https://doi.org/10.1039/c1ja10172b.

Peng, H., Yin, C., He, Q.L., et al., 2022. Development characteristics and petroleum geological significance of Permian pyroclastic flow volcanic rocks in Western Sichuan Basin, SW China. Petrol. Explor. Dev. 49 (1), 64–77. https://doi.org/10.1016/S1876-3804(22)60005-3.

Petersen, H.I., Sanei, H., Gelin, F., et al., 2020. Kerogen composition and maturity assessment of a solid bitumen-rich and vitrinite-lean shale: Insights from the Upper Jurassic Vaca Muerta shale, Argentina. Int. J. Coal Geol. 229, 103575. https://doi.org/10.1016/j.coal.2020.103575.

Qiu, N., Chang, J., Zhu, C., et al., 2022. Thermal regime of sedimentary basins in the Tarim, Upper Yangtze and North China Cratons, China. Earth Sci. Rev. 224, 103884. https://doi.org/10.1016/j.earscirev.2021.103884.

Qiu, N., Liu, W., Fu, X., et al., 2021. Maturity evolution of Lower Cambrian Qiongzhusi formation shale of the Sichuan Basin. Mar. Petrol. Geol. 128, 105061. https://doi.org/10.1016/j.marpetgeo.2021.105061.

Shellnutt, J.G., 2014. The Emeishan large igneous province: A synthesis. Geosci. Front. 5 (3), 369–394. https://doi.org/10.1016/j.gsf.2013.07.003.

Shellnutt, J.G., Pham, T.T., Denyszyn, S.W., et al., 2020. Magmatic duration of the Emeishan large igneous province: insight from northern Vietnam. Geology 48 (5), 457–461. https://doi.org/10.1130/G47076.1.

Schmidt, J.S., Menezes, T.R., Souza, I.V.A.F., et al., 2019. Comments on empirical conversion of solid bitumen reflectance for thermal maturity evaluation. Int. J. Coal Geol. 201, 44–50. https://doi.org/10.1016/j.coal.2018.11.012.

Sclater, J.G., Christie, P.A.F., 1980. Continental stretching: An explanation of the post-mid-cretaceous subsidence of the central North Sea Basin. J. Geophys. Res. Solid Earth 85 (B7), 3711–3739. https://doi.org/10.1029/JB085iB07p03711.

Sun, Z.M., Zhang, R.Q., Sun, W., et al., 2021. Petroleum exploration domains and favorable directions of the lower marine assemblage in Eastern Sichuan Basin. Geoscience 35 (3), 798–806. (in Chinese). https://doi.org/10.19657/j.geoscience.1000-8527.2021.041.

Sweeney, J.J., Burnham, A.K., 1990. Evaluation of a simple model of vitrinite reflectance based on chemical kinetics. AAPG Bull. 74 (10), 1559–1570. https://doi.org/10.1306/0C9B251F-1710-11D7-8645000102C1865D.

Tang, X.Y., Zhang, C.G., Liang, J.S., et al., 2013. Influence of igneous intrusions on the temperature field and organic maturity of the Changchang Sag, Qiongdongnan Basin, South China Sea. Chin. J. Geophys. 56 (1), 159–169. (in Chinese). https://doi.org/10.6038/cjg20130116.

Vermeesch, P., 2010. HelioPlot, and the treatment of overdispersed (U-Th-Sm)/He data. Chem. Geol. 271 (3–4), 108–111. https://doi.org/10.1016/j.chemgeo.2010.01.002.

Vermeesch, P., 2018. IsoplotR: A free and open toolbox for geochronology. Geosci. Front. 9 (5), 1479–1493. https://doi.org/10.1016/j.gsf.2018.04.001.

Wang, D., Wang, Z., Wang, T., et al., 2024. Unraveling the early Paleozoic tectonic history of the South Qinling belt: Evidence from geochronology, geochemistry, and Sm-Nd isotopes of meta-sedimentary rocks. J. Geochem. Explor. 257, 107362. https://doi.org/10.1016/j.gexplo.2023.107362.

Wang, W.Y., Pang, X.Q., Wang, Y.P., et al., 2022. Hydrocarbon expulsion model and resource potential evaluation of high-maturity marine source rocks in deep basins: Example from the Ediacaran microbial dolomite in the Sichuan Basin, China. Petrol. Sci. 19 (6), 2618–2630. https://doi.org/10.1016/j.petsci.2022.11.018.

Wang, Y., Li, M., 2021. The interaction between mantle plumes and lithosphere and its surface expressions: 3-D numerical modelling. Geophys. J. Int. 225 (2), 906–925. https://doi.org/10.1093/gji/ggab014.

Wu, J., Luo, Q., Zhang, Y., et al., 2023a. The organic petrology of vitrinite-like maceral in the lower Paleozoic shales: Implications for the thermal maturity evaluation. Int. J. Coal Geol. 274, 104282. https://doi.org/10.1016/j.coal.2023.104282.

Wu, J.H., He, L.J., Yan, L.W., et al., 2023b. Numerical simulation study on the thermal effect of Emeishan basaltic magma in the Sichuan Basin. J. Geophys. 66 (12), 5074–5085. (in Chinese). https://doi.org/10.6038/cjg2023R0148.

Xiao, B., Xiong, L., Zhao, Z., et al., 2023. Late Ordovician-early Silurian extension of the northern margin of the Upper Yangtze Platform (South China) and its impact on organic matter accumulation. J. Petrol. Sci. Eng. 220, 111238. https://doi.org/10.1016/j.petrol.2022.111238.

Xu, Y., Zheng, L., Yang, Z., et al., 2021a. Rapid eruption of the Emeishan continental flood basalts: new paleomagnetic and geochronologic constraints. Geol. Soc. Am. Bull. 134 (7–8), 1845–1862. https://doi.org/10.1130/B36132.1.

Xu, Q., Li, L., Tan, X., et al., 2021b. Middle Triassic sedimentary evolution in the Upper Yangtze region with implications for the collision between the South and North China blocks. J. Asian Earth Sci. 222, 104974. https://doi.org/10.1016/j.jseaes.2021.104974.

Xu, Q., Qiu, N., Liu, W., et al., 2018. Thermal evolution and maturation of Sinian and Cambrian source rocks in the central Sichuan Basin, Southwest China. J. Asian Earth Sci. 164, 143–158. https://doi.org/10.1016/j.jseaes.2018.06.015.

Yamada, R., Murakami, M., Tagami, T., 1995. Annealing kinetics of fission tracks in zircon: an experimental study. Chem. Geol. 122 (1), 249–258. https://doi.org/10.1016/0009-2541(95)00006-8.

Yamada, R., Murakami, M., Tagami, T., 2007. Statistical modelling of annealing kinetics of fission tracks in zircon; Reassessment of laboratory experiments. Chem. Geol. 236 (1–2), 75–91. https://doi.org/10.1016/j.chemgeo.2006.09.002.

Yuan, Y.S., Sun, S.D., Li, S.J., et al., 2013. Caledonian erosion thickness reconstruction in the Sichuan Basin. Chinese J. Geol. 48 (3), 581–591. (in Chinese). https://doi.org/10.3969/j.issn.0563-5020.2013.03.001.

Zhao, L., Mao, W., Liu, Z., et al., 2023. Research on the differential tectonic-thermal evolution of Longmaxi shale in the southern Sichuan Basin. Adv. Geo-Energy Res. 7 (3), 152–163. https://doi.org/10.46690/ager.2023.03.02.

Zhang, B., Yao, S., Ma, A., et al., 2022. New geochemical constraints on the development of active continental margin in Southeast China during the middle Permian and its tectonic implications. Gondwana Res. 103, 458–472. https://doi.org/10.1016/j.gr.2021.11.001.

Zhang, A.Q., Guo, Z., Afonso, J.C., et al., 2024. Mantle plume-lithosphere interactions beneath the emeishan large igneous Province. Geophys. Res. Lett. 51, e2023GL106973. https://doi.org/10.1029/2023GL106973.

Zheng, Z.H., Li, D.H., Bai, S.S., et al., 2017. Resource potentials of natural gas in Sichuan basin. China Petrol. Explor. 22 (3), 12–20. (in Chinese). https://doi.org/10.3969/j.issn.1672-7703.2017.03.002.

Zhu, C.Q., Hu, S.B., Qiu, N.S., et al., 2018. Geothermal constraints on Emeishan mantle plume magmatism: Paleotemperature reconstruction of the Sichuan Basin, SW China. Int. J. Earth Sci. 107 (1), 71–88. https://doi.org/10.1007/s00531-016-1404-2.

Zhu, C.Q., Qiu, N.S., Cao, H.Z., et al., 2017. Tectono-thermal evolution of the eastern Sichuan basin: constraints from the vitrinite reflectance and apatite fission track data. Earth Sci. Front. 24 (3), 94–104. (in Chinese). https://doi.org/10.13745/j.esf.2017.03.008.

Zhu, C.Q., Xu, M., Shan, J.N., et al., 2009. Quantifying the denudations of major tectonic events in Sichuan basin: constrained by the paleothermal records. Geol. China 36 (6), 1268–1277. (in Chinese). https://doi.org/10.12029/gc20090608.

Zhu, C.Q., Xu, M., Yuan, Y.S., et al., 2010. Paleo-geothermal response and record of the effusing of Emeishan basalts in Sichuan Basin. Chin. Sci. Bull. 55, 949–956. https://doi.org/10.1007/s11434-009-0490-y.

Zhu, C.Q., Xu, T., Qiu, N.S., et al., 2022. Distribution characteristics of the deep geothermal field in the Sichuan Basin and its main controlling factors. Front. Earth Sci. 10, 820456. https://doi.org/10.3389/feart.2022.824056.

Zhu, J., Zhang, Z., Santosh, M., et al., 2021. Submarine basaltic eruptions across the Guadalupian-Lopingian transition in the Emeishan large igneous province: implication for end-Guadalupian extinction of marine biota. Gondwana Res. 92, 228–238. https://doi.org/10.1016/j.gr.2020.12.025.